BNL-114374-2017-JA

Tuning Selectivity of CO2 Hydrogenation Reactions at the Metal/Oxide Interface

S. Kattel

Submitted to Journal of the American Chemical Society

July 2017

Chemistry Department

Brookhaven National Laboratory

U.S. Department of Energy
USDOE Office of Science (SC),
Basic Energy Sciences (BES) (SC-22)

DISCLAIMER

Tuning Selectivity of CO_2 Hydrogenation Reactions at the Metal/Oxide Interface

Shyam Kattel[1*], Ping Liu[1*], and Jingguang G. Chen[1,2*]

1 Chemistry Department, Brookhaven National Laboratory, Upton, New York 11973, United States

2 Department of Chemical Engineering, Columbia University, New York, New York 10027, United States

Corresponding Authors: skattel@bnl.gov, pingliu3@bnl.gov, jgchen@columbia.edu

Abstract

The chemical transformation of CO_2 not only mitigates the anthropogenic CO_2 emission into the earth's atmosphere but also produces carbon compounds that can be used as precursors for the production of chemicals and fuels. The activation and conversion of CO_2 can be achieved on multifunctional catalytic sites available at the metal/oxide interface by taking advantage of the synergy between the metal nanoparticles and oxide support. Herein, we reviewed the recent progress in mechanistic studies of CO_2 hydrogenation to C1 (CO, CH_3OH and CH_4) compounds on metal/oxide catalysts. On the basis, we were able to provide better understanding of the complex reaction network, grasp the capability of manipulating structure and combination of metal and oxide at the interface in tuning selectivity, and finally identified the key descriptors to control the activity and in particular the selectivity of catalysts. Finally, we also discussed challenges and future research opportunities for tuning the selective conversion of CO_2 on metal/oxide catalysts.

1. Introduction

Carbon dioxide (CO_2) is one of the major components of greenhouse gases emitted into earth's atmosphere due to human activities. The increasing amount of greenhouse gases produced due to human civilization over the decades has a negative impact on climate change and ocean acidification.[1,2] Considering the negative impact of CO_2 emission in global climate change, leading CO_2 emitting countries have pledged to cut CO_2 emissions significantly in the near future to limit the temperature increase to 1.5 ^{0}C above pre-industrial levels. In doing so, the rate of the atmospheric CO_2 emission is forecasted to be slower in the future. However, tens of thousands of tons of anthropogenic CO_2 will still be continuously emitted into the earth's atmosphere due to burning of fossil fuels for energy generations.

Among the different approaches explored for reducing CO_2, the chemical transformation of CO_2 to high calorific fuels is particularly attractive.[3-14] The conversion of CO_2 (by hydrogen) to fuels not only mitigates its emission into the earth's atmosphere but also produces commodity chemicals that can be either used as fuels or as precursors in many industrial chemical processes.[15] The chemical recycling of CO_2 to useful chemicals can be done using two different methods: (i) electrochemical reduction of CO_2[10,16-27] and (ii) thermocatalytic reduction of CO_2.[4,9,28-32] The electrochemical reduction of CO_2 to liquid fuels is achieved at room temperature while the thermocatalytic transformation of CO_2 is often carried out at high pressure and elevated temperature in the range of 200-300 ^{0}C.[29,30] In both cases catalysts play a critical role in determining the activity and selectivity of CO_2 transformation. The focus of the present Perspective is on the thermocatalytic transformation of CO_2 to C1 chemicals.

The importance of catalytic activation of CO_2 in carbon neutral energy conversion and storage using earth abundant catalytic materials has been highlighted in several recent reviews and

Perspective articles.[4,6,10,12,13,15,32-35] Daza et al.[36] summarized the various catalysts and their activities for CO_2 conversion to fuels via the reverse-water-gas-shift (RWGS) reaction. Dorner et al.[32] reviewed the modified Fischer-Tropsch (FT) catalysts in converting CO_2 to value-added hydrocarbons. Porosoff et al.[15] provided an overview of the various catalysts used for CO_2 conversion to CO, CH_3OH and light alkane and olefin. Rodriguez et al. recently highlighted the importance of the metal/oxide interface for the catalytic $CO_2 \rightarrow CH_3OH$ transformation,[33] showing that the catalytic activity for CO_2 conversion can be greatly promoted at the metal/oxide and metal/carbide interfaces. Another focus is on ways to convert CO_2 via photo-, electro- and thermo-reductions for instance by Kondratenko et al.[10] and Hu et al.[13] Finally, the reaction mechanisms were also outlined for CO_2 conversion to C1 fuels in a theoretical review by Li et al.[9]

Besides catalytic activity, the selectivity for CO_2 conversion is equally or maybe even more important in practice. To the best of our knowledge, the essential role of the metal/oxide interface for controlling the selectivity of CO_2 conversion has not been critically reviewed. The current Perspective aims to identify the general trends, as well as challenges and opportunities in designing metal/oxide interfaces to achieve selective CO_2 hydrogenation. Due to the complexity of the reaction network for CO_2 hydrogenation (Figure 1), multiple products can be formed and the separation of product can be very expensive in practical applications. The current Perspective provides a bottom-up review on how the synergistic interactions at the metal/oxide interface can tune the reaction mechanisms and in turn the selectivity of CO_2 hydrogenation. Typically the activity of the catalyst is associated with multiple catalytic sites available at the metal/oxide interface, according to recent studies using in-situ, operando experimental techniques and theoretical calculations, where bifunctional [28,37-40] and/or electronic effects [41-46] contribute to modify the bonding strength. The metal/oxide interface provides multiple sites for the adsorption

of reaction intermediates. In some cases,[28,38,47-49] the simultaneous participation of both the metal sites on metal nanoparticles and the M^+ or O^{2-} sites of oxides is observed to stabilize the key reaction intermediates, e.g. $*CO_2$, $*C_xH_y$ and $*C_xH_yO_z$ species. In this regard, the metal/oxide interface is bifunctional. The electronic effect creates unique electronic properties at the metal/oxide interface due to the strong interaction between the metal and oxide support, which can be different from that of each component and be suitable for CO_2 activation and its subsequent transformation. However, it is not straightforward to isolate these two effects which can occur simultaneously.[50,51] Here, we will focus on the catalyst selectivity, using the metal/oxide interface in determining the product selectivity of CO_2 to toward C1 carbon compounds: carbon monoxide (CO), methanol (CH_3OH) and methane (CH_4). We will first summarize the activity and reaction mechanisms of the oxide-supported metal catalysts that are selective to produce CO, CH_3OH, and CH_4. It will be followed by the discussion on the challenges and opportunities for the rational design of metal/oxide interfaces by choosing the appropriate combination of metals and oxides to achieve high activity and selectivity toward CO_2 hydrogenation.

2. CO_2 Hydrogenation to CO

CO is the simplest C1 product of the CO_2 hydrogenation through the RWGS reaction, $CO_2(g) + H_2(g) \rightarrow CO(g) + H_2O(g)$. CO is a valuable precursor molecule that can be used for CH_3OH synthesis and for the production of longer chain hydrocarbons in the FT process. Various metals including precious metals Pt,[52-55] Pd,[56] Rh[57] and Au[58,59] and non-precious metals Cu,[60-66] Fe[67] and Ni[68-71] supported on oxides were reported to be active towards the production of CO (Table 1). Cu was one of the extensively studied metal catalysts for the RWGS reaction, whose catalytic activity for CO_2 hydrogenation was found to be sensitive to its dispersion, surface morphology and particle size.[60,65,66] For example, highly dispersed Cu nanoparticles on the ZnO

support showed high activity for CO_2 hydrogenation reaction to produce CO.[72] Pt was also widely studied as a catalyst for promoting the RWGS reaction to produce CO. The activity and selectivity of Pt catalysts were found to be influenced by the nature of the oxide support. For example, Pt/γ-Al_2O_3 was less active and more selective to CO than Pt/CeO_2 at similar Pt loadings and CO_2 conversion.[73] Rh was another active metal for the RWGS reaction when deposited on different supports (MgO, Nb_2O_5, ZrO_2 and TiO_2, Table 1).[36,57,74,75] Rh/TiO_2 with low Rh loadings was selective to CO,[75] where the RWGS activity was higher than the CO_2 methanation activity at 200 ^{0}C for two different ratios of CO_2:H_2 (Figure 2). Furthermore, a quantitative site-specific correlation between CO and CH_4 selectivity on Rh/TiO_2 was reported using diffuse reflectance infrared Fourier transform spectroscopy (DRIFTS) measurements. It was proposed that the RWGS reaction only occurred at isolated Rh atomic sites while the CO_2 methanation reaction was on Rh atoms interacted with Rh nanoparticles[75] Bimetallic catalysts such as PtNi, PtCo and PdNi were also studied for CO_2 hydrogenation to CO.[73,76] Results in Table 2 showed that bimetallic catalysts displayed higher activity and CO selectivity than the individual monometallic catalysts deposited on the same oxide supports.[73]

CO_2 hydrogenation to CO via the RWGS reaction, can proceed via the carboxyl (*HOCO) intermediate (Figure 1). Alternatively, *CO_2 can dissociate into *CO + *O via the direct C-O bond cleavage pathway, and formed *CO can desorb as a product CO(g). Density functional theory (DFT) calculations showed that CO_2 was activated and bound at the metal/oxide interface via a configuration with C atom of *CO_2 bound to the metal site and one of the O atoms of CO_2 bound to the metal cation (M^+) of the oxide support for various oxide supports e. g. SiO_2, Al_2O_3, TiO_2, CeO_2, ZrO_2, In_2O_3 and ZnO.[28,38,47-49,77-80] The dissociation of molecular H_2 occurred relatively easily on the metal sites, and the spillover of hydrogen atoms from metal sites to oxide supports,

e.g. SiO_2, TiO_2, ZrO_2, was also observed, which formed hydroxylated oxide surfaces.[81,82] In some cases, e. g. Pt/SiO_2,[51] Cu/TiO_2,[38] $*CO_2$ underwent hydrogenation and formed *HOCO, which dissociated to produce *CO either at the metal or metal/oxide interfacial sites. The relatively stronger binding of *HOCO was necessary for its dissociation with a low activation energy. In other cases, e.g. Cu/ZrO_2,[48] $*CO_2$ preferred dissociation reaction over its hydrogenation according to the DFT and kinetic Monte Carlo (KMC) study.

The nature of oxide supports influence the activity of metal/oxide catalysts toward CO_2 conversion via the direct participation in CO_2 binding. In term of activity, the reducibility of oxide is important,[55] and the presence of an O-vacancy provided the site for CO_2 adsorption which is otherwise a difficult step.[83-87] On Pt/SiO_2, a non-reducible support, O vacancies were difficult to be formed and CO_2 bound weakly at the Pt-SiO_2 interface; in contrast, the presence of an O vacancy on TiO_2, a reducible support, provided much stronger binding for CO_2 (Figure 3).[51] The stronger binding of CO_2 on Pt/TiO_2 compared to Pt/SiO_2 was likely responsible for the experimentally observed higher activity of CO_2 conversion to CO on Pt/TiO_2.[51] The effect on selectivity rather depend on the binding of CO.[28,88,89] A similar CO selectivity was observed on both Pt/TiO_2 and Pt/SiO_2, because on both catalysts CO primarily interacted with Pt, and the similarity in CO binding energy. Besides Pt/oxides, the importance of CO binding in determining CO selectivity was also observed for Pt alloy/oxides and Cu/oxides.[38,39] A combination of ambient pressure X-ray photoelectron spectroscopy (APXPS) and DFT calculations for the model surfaces and transmission electron microscopy (TEM), Fourier transform infrared (FTIR) spectroscopy, DRIFTS, and extended X-ray absorption fine structure (EXAFS) analysis for the corresponding powder catalysts showed that changing the support from TiO_2 to CeO_2 and ZrO_2 did not affect the CO_2 hydrogenation pathway of the PtCo alloy; however, CO selectivity was greatly influenced.[39]

Figure 4 shows the FTIR spectra recorded during CO_2 hydrogenation on the PtCo/oxides catalysts. The vibrational modes ν(C=O) at 2358 cm^{-1}, ν(C≡O) at 2170 cm^{-1}, and ν(C-H) at 3016 cm^{-1} were used to monitor the presence of CO_2, CO, and CH_4, respectively. On $PtCo/TiO_2$, a sharp band corresponding to CO was detected (Figure 4a) while on $PtCo/CeO_2$, vibrational peaks corresponding to the formation of CH_4 were observed in addition to the peaks corresponding to CO. Even though CO was observed as a product on both $PtCo/TiO_2$ and $PtCo/CeO_2$ model and powder catalysts, $PtCo/TiO_2$ was found to selectively promote $CO_2 \rightarrow CO$ conversion because of weak CO binding at the $PtCo/TiO_2$ interface. In addition, both DFT calculations and experiments using the steady state flow reactor demonstrated that Cu/TiO_2 was more selective for CO production than Cu/ZrO_2.[38] This was associated with the weakened interaction of *CO at the Cu/TiO_2 interface compared to the Cu/ZrO_2 interface.

Overall, the previous studies on Pt, Cu/oxide catalysts shined the light on the principles to tune the activity and selectivity of metal/oxide catalysts during CO_2 hydrogenation to CO. The promotion in activity required the strengthened interaction to CO_2 at the metal/oxide interface, being able to facilitate the overall conversion via either the RWGS or the direct C-O bond cleavage pathway. CO selectivity of a metal/oxide catalyst is primarily determined by the binding capability of the metal/oxide interface for CO.[38,39,51,90] The metal/oxide interface that binds CO weakly should be selective to CO simply because of facile desorption of *CO. Conversely, when *CO is strongly bound, its hydrogenation or dissociation is likely more favorable than desorption, and consequently the catalyst is likely to show lower CO selectivity.

3. CO_2 Hydrogenation to CH_3OH

CH_3OH synthesis from the thermocatalytic CO_2 transformation, $CO_2(g) + 3H_2(g) \rightarrow *CH_3OH(g) + H_2O(g)$, has gained tremendous interests in recent years.[28-30] Among many materials

studied, oxide-supported metals have emerged as promising catalysts and the metal/oxide interfaces have been identified to play a critical role in controlling the activity and selectivity for CH_3OH synthesis from CO_2 hydrogenation.[91,92] For example, the synergistic effect between the metal and oxide in promoting CO_2 conversion to CH_3OH was observed in Cu/oxide catalysts, surpassing the activity of Cu catalysts without oxide supports.[28,30,38,91] Pd[93-95,96-99] and Au[31,37,100] supported on oxides have also been reported to be active for CH_3OH synthesis from the CO_2 hydrogenation at moderate reaction temperature and pressures (Table 1).

$Cu/ZnO/Al_2O_3$ is an industrially used catalyst for the transformation of CO_2 to CH_3OH at high pressures (50-100 atm) and elevated temperatures (200-300 ^{0}C), [29,30,101] though CO is still the major product. Significant efforts have been made to understand the nature of the active sites in $Cu/ZnO/Al_2O_3$ for CO_2 activation and conversion.[29,30,91,102-107] Recently, the synergy between Cu and ZnO arising from the strong-metal-support-interaction (SMSI) was attributed to the formation of CuZn alloy, where Zn atoms at the step edges of Cu nanoparticles were proposed to be active sites using a combination of experimental measurements and theoretical calculations and the Zn coverage was quantitatively correlated with the methanol synthesis activity (Figure 5).[30,102] On the other hand, recent TEM studies revealed that the SMSI between Cu and ZnO led to the encapsulation of ZnO overlayers (Figure 6) over Cu particles during CH_3OH synthesis on the $Cu/ZnO/Al_2O_3$ catalyst, which could potentially create new catalytically active sites.[101,103] Indeed, the combined X-ray photoemission spectroscopy (XPS) measurements, DFT calculations and kinetic Monte Carlo (KMC) simulations on model ZnCu(111) catalysts showed that the CuZn alloy underwent surface oxidation under the reaction conditions and the surface Zn was transformed into ZnO, creating a catalytically active Cu/ZnO interface (Figure 7) for CH_3OH synthesis.[47] In another example, the CH_3OH synthesis activity of $Cu/CeO_x/TiO_2(110)$ was found

to be ~1280 times higher than Cu(111) (Figure 8).[28] The unique Cu/CeO_x interface not only activated CO_2 but also selectively stabilized the reaction intermediates and facilitated the overall CO_2 conversion to CH_3OH with an apparent activation energy lower than Cu(111).

Pd catalysts supported on various oxides (Al_2O_3, SiO_2, TiO_2, CeO_2, Ga_2O_3, MgO and ZnO) have also been studied for CO_2 transformation to CH_3OH.[97,98,108,109] An earlier study by Erdohelyi et al.[108] showed that Pd supported on TiO_2 displayed the highest activity for CO_2 hydrogenation among Pd supported on Al_2O_3, SiO_2, TiO_2 and MgO. The selectivity of CO_2 hydrogenation on Pd/oxides catalysts was shown to largely depend on Pd particle size; CO and CH_3OH were produced on poorly dispersed Pd while CH_4 was the main product on highly dispersed Pd.[108] Pd/CeO_2 was reported to be highly selective to CH_3OH (CH_3OH selectivity ~90 %) at a temperature of 230 ºC and a pressure of 30 bar when CO_2:H_2 ratio is 1:3.[110] The SMSI effect between Pd and oxides such as CeO_2 or TiO_2 created catalytically active interfacial sites for CO_2 hydrogenation.[98,111] Fujitani et al.[94] showed that Pd/Ga_2O_3 was more active than Cu/ZnO by a factor of 2 in yield and 20 in turnover frequency for CO_2 hydrogenation. Pd/ZnO was another metal/oxide catalyst studied which showed high CH_3OH selectivity, where Pd/ZnO prepared by sol immobilization method exhibited much higher than that prepared by impregnation method for identical Pd loadings (Figure 9). [92,103,106] The promotional effect of ZnO, similar to that on Cu/ZnO, on Pd forming catalytically active Pd-Zn alloy has been proposed.[99]

Au/oxide was reported to have comparable activity in CO_2 hydrogenation as Cu/oxide in the temperature range of 150-400 °C.[31,37,100,112] Smaller Au particles were shown to give higher CH_3OH productivity.[100] The oxide supports also matter. The CH_3OH production was observed following the order of Au/ZrO_2 > Au/ZnO > Au/TiO_2 > Au/Al_2O_3 with similar Au nanoparticle size (Figure 10).[31] The catalytic performance of Au/ZnO catalyst for CH_3OH production[87,100] was

impressive given that the metal mass-normalized activity was comparable to and the selectivity for CH_3OH formation was significantly higher than (> 50% compared to 37%) those of a commercial $Cu/ZnO/Al_2O_3$ catalyst. Finally, the mixed oxide, CeO_x/TiO_2, supports was found to be able to promote the CO_2 conversion to CH_3OH at the $Au/CeO_x/TiO_2$ interface to a level comparable to those of $Cu/CeO_x/TiO_2$ catalysts.[37]

There are two major reactions pathways proposed for the production of CH_3OH from CO_2 hydrogenation based on experimental observations and theoretical calculations (Figure 1).[38,48,77,83,113-117] The first pathway is featured by the *CO intermediate, which is produced from the RWGS reaction via the carboxylate (*HOCO) species or via the direct C-O bond cleavage of $*CO_2$ and is further hydrogenated to the final product CH_3OH (designated as the RWGS + CO-Hydro pathway); the other pathway is associated with the formate (*HCOO) intermediate formed by the initial step in $*CO_2$ hydrogenation, which eventually produces CH_3OH via the C-O bond cleavage of the $*H_2COOH$ intermediate (designated as the Formate pathway). As shown in Figure 1, the CH_3OH production from both pathways involves many reaction intermediates and can occur in various possible routes. The identification of the active reaction intermediates is essential to fully explore the preferred pathways in which CO_2 is hydrogenated to CH_3OH, which requires the combination of experimental observations and theoretical calculations.[38]

The preferred pathway for the CO_2 hydrogenation is primarily controlled by the binding capability of the catalyst with the key reaction intermediates.[38] As shown in Figure 11, the metal/oxide (e.g. Cu/TiO_2) interface directly participates in binding and stabilizing of the reaction intermediates. The initial hydrogenation of CO_2 determines the pathway for CO_2 hydrogenation. In general, at the metal/oxide interface, *HCOO along the Formate pathway adsorbs through two O atoms in the bidentate configuration (Figure 11d), while *HOCO along the RWGS pathway

binds through a single O atom (Figure 11c). Consequently, the stability of *HCOO is mostly higher than that of *HOCO and the barrier for the formation of *HCOO is expected to be lower than that for the formation of *HOCO.[38] This was the case for Cu/ZnO where the Formate pathway was preferred over the RWGS + CO-Hydro pathway for CH_3OH production.[30,47] Along the Formate pathway, the hydrogenation of *HCOO to *HCOOH and *H_3CO hydrogenation to *CH_3OH displayed the highest barrier among the elementary steps according to the DFT calculations.[47] That is, the interaction of *HCOO with the surface can be one of the keys to facilitate CH_3OH production along the Formate pathway, being strong enough to facilitate CO_2 hydrogenation, but weakly enough to allow further hydrogenation.

The over stabilization of the *HCOO species can result in surface poisoning of metal/oxide catalysts over time, which hinders the Formate pathway.[28,38] DFT calculations (Figure 12) and KMC simulations performed at experimental reaction conditions on Cu/TiO_2 and Cu/ZrO_2 catalysts predicted the poisoning of catalysts due to accumulation of surface *HCOO species during CO_2 hydrogenation.[38] On Cu/TiO_2, Cu/CeO_2 and Cu/ZrO_2, *HCOO acted as a spectator, and the CH_3OH production did not occur via the Formate pathway..[28,38] Under such situation, the CH_3OH formation can occur via the *HOCO intermediate along the RWGS + CO-Hydro pathway.[28,38] For Cu/oxide catalysts, in particular, the binding strength of *CO to the catalysts was again critical to the production of CH_3OH, similar to that of CO production (see Section 2).[38,90] The main difference is that the conversion to CH_3OH requires a catalyst that binds *CO strongly enough to enhance its hydrogenation to formyl species (*HCO), rather than its desorption.[38] Besides, the stability of *HCO, *H_2CO and *H_3CO intermediates is also important. An ideal Cu/oxide catalyst for $CO_2 \rightarrow CH_3OH$ conversion via the RWGS + CO-Hydro pathway should promote the initial hydrogenation of *CO_2 to *HOCO and simultaneously stabilize the *CO,

*HCO and *H_2CO active intermediates, while *H_3CO should be destabilized to allow its hydrogenation to CH_3OH. Herein, the reduced $M^{\delta+}$ sites at the metal/oxide interface can play a critical role in stabilizing the *CO, *HCO and *H_2CO intermediates through a $M^{\delta+}$-O interaction. Indeed, a combined theory-experiment study showed that upon going from Cu/TiO_2 to Cu/ZrO_2, the CO_2 conversion was facilitated due to the fine-tuning capability of ZrO_2, being strong enough to stabilize *CO_2, *CO, *HCO, and *H_2CO at the Cu/ZrO_2 interface and therefore to promote its hydrogenation to CH_3OH via the RWGS + CO-Hydro pathway, but weak enough to prevent the poisoning of the active sites.[38]

The variation in the size of metal nanoparticles also affects the selectivity. The Cu_4/hydroxylated-Al_2O_3 model catalyst showed high activity for CO_2 conversion to CH_3OH at a low CO_2 partial pressure.[117] According to DFT calculations, the CO_2 hydrogenation on Cu_4/Al_2O_3 was highly selective to CH_3OH via the Formate pathway; by comparison the production of CO or CH_3OH along the RWGS reaction was kinetically less favorable (Figure 13).[117] The unique coordination environment of Cu atoms in small Cu clusters on Al_2O_3 was able to tune the bindings of Cu with reaction intermediates, leading to the selective production of CH_3OH.

The mechanistic studies of Cu/oxide catalysts indicated that the conversion of CO_2 to CH_3OH can proceed via both the Formate and the RWGS + CO-Hydro pathways. Along the Formate pathway, the binding of *HCOO is important, which should be tuned being able to promote the hydrogenation of *CO_2 to *HCOO, but not over-stabilized to prevent surface poisoning. In term of selectivity, *H_3CO should be destabilized on the surface to allow the production of CH_3OH. By comparison, the situation along the RWGS + CO-Hydro pathway is more complex. To achieve high activity, the metal/oxide interfacial sites should selectively provide stabilization to *CO_2 and facilitate *HOCO formation. To enhance CH_3OH selectivity, the

bindings of *CO, *HCO, and *H_2CO should be increased, while that of *H_3CO should be decreased. For such complex reaction network, the binding energy of a single intermediate, or single descriptor, may not be adequate enough to well describe the catalytic performance; instead it is likely controlled by several key species, which work in a cooperative way. The binding strength of adsorbates on the catalysts can be tuned by selecting different metal/oxide catalysts and by controlling the metal particle size. The combination of DFT calculations, KMC simulations, and experimental measurements is essential to provide significant insight into the complex reaction mechanisms of CO_2 hydrogenation to CH_3OH.

4. CO_2 Hydrogenation to CH_4

Converting CO_2 to CH_4 by H_2, or CO_2 methanation, $CO_2(g) + 4H_2(g) \rightarrow CH_4(g) + 2H_2O(g)$, is a promising way to produce synthetic natural gas. As summarized in Table 1, Ni catalysts supported on various oxides, SiO_2,[118,119] Al_2O_3,[120-123] TiO_2,[124] CeO_2,[125-127] and ZrO_2[127,128] have been shown to promote the CO_2 methanation reaction. The activity of Ni-based catalysts for CO_2 methanation was found to be promoted by the addition of second metals or other oxides.[93,129,130] For example, the synergy between the precious metals Rh or Ru and Ni was observed on both activity and selectivity of Ni based $Ce_xZr_{1-x}O_2$ catalysts.[129] Furthermore, Ni loading also played a major role in both activity and selectivity for CO_2 methanation. A recent experimental study showed that both CO_2 conversion and CH_4 selectivity of Ni/γ-Al_2O_3 catalyst were affected by Ni content and 20 wt.% of Ni loading showed the highest activity and selectivity.[120] Ru[130-140] and Rh[75,141] supported on oxides (Table 1) were also widely studied. HRSTEM and XPS measurements on Ru/TiO_2 catalysts showed encapsulation of Ru particles by the TiO_2 support due to the SMSI. Time-resolved in-situ EXAFS measurements showed that the presence of H_2O increased the CH_4 selectivity of Ru/TiO_2 catalysts due to the promotion of the OH group for CO_2 adsorption and

dissociation.[142] Ru-doped CeO_2 showed a higher selectivity for CO_2 methanation reaction than that of doping Ni, Co or Pd.[131] The promoting effect of adding a secondary oxide or metal component on the overall rate was also observed for Ru/Al_2O_3 with the addition of CeO_2[130] and Pd/SiO_2 with addition of Mg,[93] respectively.

The possible pathways for CO_2 hydrogenation to CH_4 are summarized in Figure 1.[39,51,124,132,139,140,143-145] The CH_4 formation can occur via the Direct C-O bond cleavage, the RWGS + CO-Hydro and Formate pathways. Along the Direct C-O bond cleavage pathway, $*CO_2$ dissociates to *CO and *O and the produced *CO undergoes dissociation reaction to form *O and *C, which is subsequently hydrogenated to CH_4.[143] Alternatively, *CO may be hydrogenated to *HCO, which dissociates to *CH + *O and *CH is hydrogenated to CH_4.[124] Along the RWGS + CO-Hydro pathway the C-O bond scission of *HCOH, $*H_2COH$ or $*H_3CO$ leads to the formation of CH_x species which undergo subsequent hydrogenation reactions to form CH_4.[39,51] Along the Formate pathway, CH_4 formation occurs via the C-O bond cleavage in H_2COH or H_3CO.[51] The CH_4 selectivity is therefore ultimately determined by the competition between C-O bond scission in H_xCO species and their hydrogenation reactions.[39,51] Thus along all three pathways, the C-O bond scission of the H_xCO species is a critical step and likely determines the overall CH_4 selectivity in CO_2 hydrogenation.

Compared to mechanistic studies for CO and CH_3OH productions on metal/oxide catalysts, much less attention has been paid to CH_4 production. On $Ni/\gamma\text{-}Al_2O_3$ catalysts, the kinetics of CO_2 methanation was found to follow the Direct C-O bond cleavage pathway in which the rate-limiting step was the subsequent dissociation of adsorbed *CO.[121] The detailed mechanisms of CO_2 methanation on Ru(0001) was studied by combined DFT calculations and microkinetic modeling.[146] It was found that the CH_4 production primarily occurred via the direct $*CO_2$

dissociation to *CO + *O followed by several steps: hydrogenation of *CO to *HCO, *HCO dissociation to *CH + *O, and *CH hydrogenation to *CH_4. The reaction of *HCO dissociation to *CH + *O was predicted to be the rate-liming step. The mechanism of CH_4 formation on Pt/oxide and Cu/oxide catalysts was well described, though the catalysts were highly selective to CO or CH_3OH.[51,117] The addition of a secondary Co component on Pt/CeO_2 or Pt/ZrO_2 tuned the selectivity more toward CH_4 than that without Co, though CO was still the major product.[39] According to DFT calculations, CH_4 formation occurred via the RWGS reaction via the *H_3CO intermediate at the PtCo/oxide interface (Figure 14).[39] The DFT prediction of the presence of the H_3CO intermediate as a precursor for the formation of CH_4 on PtCo/oxides, such as $PtCo/ZrO_2$,was also confirmed in the corresponding experiments.[39] As shown in Figure 13, *H_3CO was also a precursor for the C-O bond cleavage for the production of CH_4 on Cu_4/Al_2O_3; however, the C-O bond cleavage could not compete with the hydrogenation of *H_3CO, as a result CH_3OH was the major product of CO_2 hydrogenation.[117]

In general, on a metal/oxide catalyst, several of the steps involved in CO_2 methanation are similar to the steps in the RWGS + CO-Hydro and Formate pathways for the formation of CH_3OH. The selectivity of CO_2 hydrogenation towards CH_3OH or CH_4 is primarily determined by the competition between the pathways of C-O bond scission and the hydrogenation of H_xCO species. To tune the selectivity of metal/oxide catalysts toward CH_4 rather than CH_3OH during CO_2 hydrogenation, metal/oxide interfaces should strengthen the binding for H_xCO species to facilitate the C-O bond scission.

5. Conclusions, Challenges and Future Opportunities

The chemical transformation of CO_2, however challenging because of its high thermochemical stability, is one of the potential ways to utilize CO_2 and to store energy in the form

of chemical energy. Recent progress made based on experimental and atomistic theoretical simulations have shown that CO_2 can be activated and subsequently hydrogenated to C1 carbon compounds on metal/oxide catalysts by utilizing multifunctional catalytic sites available at the metal/oxide interface.[28,38,39] It has been shown that the binding strengths of key reaction intermediates at the metal/oxide interface determine the reaction pathways and selectivity in CO_2 hydrogenation reactions. Oxides are found to be able to promote CO_2 conversion to CO and/or CH_3OH on the supported Au, Pd, Cu catalysts at moderate temperatures and pressures.[28-30,38] The combination of oxide with Pt tunes the selectivity toward the production of CO. When Ni[118,121-123,126-128,143,147,148] or Ru[124,130,131,134,136] particles are deposited on oxides, $CO_2 \rightarrow CH_4$ conversion is selectively promoted. Furthermore, the additions of a secondary oxide or metal component, as well as the variations in metal or oxide particle size, also demonstrate the potential in tuning the binding strengths of key intermediates at the metal/oxide interface and consequently the selectivity for CO_2 hydrogenation.

The production of CO proceeds following the RWGS reaction via *HOCO intermediate and/or the direct C-O bond cleavage pathways (Figure 1), where the binding strength of CO_2 at the metal/oxide interface is likely the key to determine the preferred pathway.[38,39,48,51] The CO selectivity is controlled by the CO binding energy. On both Pt/oxide and Cu/oxide systems, the RWGS is preferred and the CO binding is weak enough to enable facile desorption of *CO rather than its hydrogenation or dissociation under reaction conditions. For CH_3OH synthesis, two possible reaction routes are proposed (Figure 1).[30,38,39,48,51,90,113,149,150] The first pathway is featured by the *CO intermediate from the RWGS reaction and is further hydrogenated to the final product CH_3OH; the other pathway is associated with the *HCOO intermediate formed by the initial step in CO_2 hydrogenation, which eventually produces CH_3OH via the C-O bond cleavage of the

*H_2COOH intermediate. Depending on the oxides used, the preferred reaction pathway can go from the Formate pathway on Cu/ZnO,[30,47] to the RWGS + CO-Hydro pathway on Cu/CeO_2,[28] Cu/TiO_2 and Cu/ZrO_2,[38] where the Formate pathway is hindered for CH_3OH production due to the accumulation of strongly bound *HCOO species on the surface.[38] Thus ideally, the binding property of Cu/oxide catalysts should be tuned selectively, improving the stability of *CO_2, *CO, *HCO, and *H_2CO while destabilizing *HCOO and*H_3CO, to achieve a high selectivity toward CH_3OH. The CH_4 selectivity is associated with the Direct C-O bond cleavage, the RWGS + CO-Hydro or Formate pathways (Figure 1), where the Direct C-O bond cleavage is identified for Ru-based catalysts.[39,117,124,143] The CH_4 selectivity is likely determined by the competition between the hydrogenation and C-O bond scission reactions of the *H_xCO intermediates.[51] To achieve high CH_4 selectivity, the binding of *H_xCO species should be strong enough to facilitate the C-O bond cleavage. Overall, the formation of any of the three C1 products involves complex reaction network and catalyst. Therefore, the binding energy of a single intermediate, or a single descriptor, may not be adequate to well describe the catalytic performance; instead it is likely controlled by several key species that work in a cooperative way.

The selective conversion of CO_2 to C1 compounds at the metal/oxide interface of oxide-supported metal catalysts offers challenging research opportunities in the following areas:

(1) *Understanding reaction pathways for CO_2 conversion under realistic conditions*. Although oxide-supported metal materials are widely studied as catalysts for CO_2 hydrogenation reaction,[28,30,38,39,101,103] there are very limited comprehensive studies utilizing in-situ/operando experimental techniques and theoretical simulations at relevant experimental reaction conditions on the reaction mechanisms and key steps that control the activity and selectivity. Such atomic level understanding is essential

for the realization of a better catalyst by design. At present possible pathways for CO_2 conversion are proposed primarily based on DFT calculations.[30,48,113-116] Future experimental measurements should focus on identifying the active reaction intermediates using in-situ spectroscopic techniques. Meanwhile, theoretical simulations should be performed at experimental reaction conditions using more realistic models, where the combination of KMC or microkinetic simulations with DFT calculations is necessary.[38,51,113,115]

(2) *Theoretical modeling of metal/oxide interfaces to minimize the gap between theory and experiments.* Current DFT calculations about CO_2 conversion, due to their intense computational demand, are often performed using small metal clusters of less than 1 nm.[37,48,51,77] However, the average particle size in experimentally synthesized catalysts is typically larger and is of the order of several nm.[39,73] Given that the particle size could play a major role in CO_2 conversion with different activity and selectivity,[75] future theoretical calculations should minimize this gap by using models relevant to experiments. In this aspect, the cooperation between the in-situ experimental measurements and theoretical calculations on both model surfaces and powder catalysts is essential to shed light on the possible reaction routes for the complex CO_2 conversion at the metal/oxide interface.

(3) *Identifying descriptors of activity and selectivity for CO_2 conversion.* Despite numerous studies,[38,48,51,90,113,116,117,149,150] those aiming to identify the descriptors for CO_2 conversion at the metal/oxide interface, especially for selectivity, are still limited. The descriptors for CO_2 hydrogenation to CO, CH_4 and CH_3OH on transition metal surfaces have been proposed using analytical approaches based on the DFT

microkinetic modeling.[146,151] It was shown that the selectivity of catalytic CO_2 hydrogenation to CO and CH_4 on the transition metal catalysts could correlate well with the oxygen binding energy: weaker oxygen binding metals only converted CO_2 mildly to CO, whereas stronger oxygen binding metals enabled more deep conversion to CH_4.[146] Even though some progress has been made in identifying the descriptors of selectivity in CO_2 hydrogenation on transition metal surfaces, it remains a challenge in identifying such descriptors for catalytic systems that explicitly include nanoscale effects that are introduced via size and shape or oxide supports. Therefore, systematic theoretical studies, similar to what has been successfully done for other reactions such as oxygen reduction reaction (ORR),[152,153] oxygen evolution reaction (OER)[89,154] etc, should be carried out toward the identification of universal descriptors. The descriptor-based catalyst screening could potentially help find the next generation of highly active and selective catalysts for CO_2 transformation. The CO_2 hydrogenation is much more complex in kinetics than ORR and OER. Therefore, descriptors can be associated with a variety of reaction intermediates and the optimal performance may require the complex coordination between different descriptors.

(4) *Tuning the activity and selectivity in CO_2 conversion using promoters.* The promoters can help tune the activity and selectivity of CO_2 hydrogenation.[38,39,90] A promoter can be a defect site, a doped metal component, the adsorbed surface species (e.g. *O and *H), the deposited/grown nanostructures (e.g. oxide nanoparticles and thin films), etc. on the existing catalysts. The presence of such promoter is able to enhance the catalytic activity/selectivity of the CO_2 hydrogenation reaction. In particular, the effect of promoters on the currently working catalysts should be considered, e.g. bimetallic

alloys, defects, dopants and mixed oxide supports. The incorporation of promoters could lead to the discovery of selective and active catalysts. The future experimental studies, therefore, should focus on controlled synthesis of promoters incorporated into the oxide-supported metal catalysts. Complementary to the experimental studies, theoretical modeling should be performed on promising catalysts to elucidate how the the rate and selectivity controlling steps are affected by the promoters.

(5) *Synthesizing catalysts with optimized metal/oxide interfaces.* The size of metal nanoparticles deposited on oxide supports, which most likely determines true nature of the metal/oxide interface, has been shown to influence the activity and selectivity of CO_2 hydrogenation.[75] For example, the CO selectivity of sol-immobilized Pd/ZnO catalysts increased from 40 to 80% with the PdZn particle size increasing from 3 to 7 nm at 250 ^{0}C and 20 bar.[99] In contrast, the intrinsic CO_2 methanation activity of Rh/γ-Al_2O_3 catalysts with particle size in the range 3.6 to 15.4 nm did not appear to depend on particle size at temperatures between 185 to 200 ^{0}C, whereas at lower temperatures larger particles favored higher activity.[155] CO_2 hydrogenation studied using Co nanoparticles supported on SiO_2 showed an increase of the turnover frequency with increasing average particle size from 3-10 nm, however, the selectivity was independent of the particle size.[156] For CO_2 hydrogenation to CH_3OH on Au/ZnO catalysts, it was found that the activity increased while the selectivity decreased with decreasing particle size from ~3-10 nm. A similar trend in activity was observed on Cu/Al_2O_3 catalysts for CO_2 to CH_3OH transformation.[78] Thus, controlling particle morphology, size and dispersion may also help in optimizing the metal/oxide interface and consequently tuning selectivity. The optimized metal/oxide interface can be in

various forms. It is known that the selectivity for CO_2 hydrogenation to CO, CH_3OH and CH_4 depends on many factors: e. g. size, morphology and dispersion of deposited metal particles, nature of oxide supports, etc. For example, the selective transformation of CO_2 to CH_3OH on the Cu/oxide catalysts requires well dispersed subnanometer Cu particles deposited on oxide supports.[78,117] Future research in this area should be directed at identifying an optimized combination of metal and oxide support that selectively promotes CO_2 to CO, CH_3OH or CH_4. Once such combination is identified, the selectively could potentially be further enhanced via tuning the particle size and the dispersion of deposited metal nanoparticles. Furthermore, the activation of CO_2 typically occurs at the metal/oxide interface with a nearby oxygen vacancy in the oxide support.[51] As a result, the reduced oxide supports heavily influence the activity and selectivity of CO_2 hydrogenation. Controlled synthesis of both metal particles and oxide substrates, using techniques such as chemical vapor deposition or atomic layer deposition, would play an important role in optimizing metal/oxide interfaces for selective CO_2 conversion.

(6) *Investigating stability of catalysts under reaction conditions.* The morphological changes and chemical transformation of the catalysts during CO_2 hydrogenations have been reported for example on $Cu/ZnO/Al_2O_3$ catalysts.[101] Another recent study has identified adsorbate-induced strong metal support interaction during CO_2 hydrogenation.[157] Any changes in the electronic and/or physical structures of the metal or oxide would modify the nature of metal/oxide interface and consequently the activity and selectivity of CO_2 conversion. Current experimental studies about the structure of the catalysts are mainly based on the ex-situ characterization techniques.

Future experimental studies should focus on in-situ monitoring of the dynamics of the catalyst structure and transformation. Such information would be extremely useful to design stable metal/oxide interface at the operating conditions of CO_2 hydrogenation.

Acknowledgements

The research was carried out at Brookhaven National Laboratory supported by the U.S. Department of Energy (DOE), Office of Science, Office of Basic Energy Sciences, Division of Chemical Sciences, Biosciences and Geosciences, under contract No. DE-SC0012704.

References

(1) Knutson, T. R.; Tuleya, R. E. *J Climate* **2004**, *17*, 3477.
(2) Hansen, J.; Sato, M.; Ruedy, R.; Lo, K.; Lea, D. W.; Medina-Elizade, M. *P Natl Acad Sci USA* **2006**, *103*, 14288.
(3) Najafabadi, A. T. *Int J Energ Res* **2013**, *37*, 485.
(4) Liu, X. M.; Lu, G. Q.; Yan, Z. F.; Beltramini, J. *Ind Eng Chem Res* **2003**, *42*, 6518.
(5) Xu, X. D.; Moulijn, J. A. *Energy & Fuels* **1996**, *10*, 305.
(6) Aresta, M.; Dibenedetto, A.; Angelini, A. *Chem Rev* **2014**, *114*, 1709.
(7) Appel, A. M.; Bercaw, J. E.; Bocarsly, A. B.; Dobbek, H.; DuBois, D. L.; Dupuis, M.; Ferry, J. G.; Fujita, E.; Hille, R.; Kenis, P. J. A.; Kerfeld, C. A.; Morris, R. H.; Peden, C. H. F.; Portis, A. R.; Ragsdale, S. W.; Rauchfuss, T. B.; Reek, J. N. H.; Seefeldt, L. C.; Thauer, R. K.; Waldrop, G. L. *Chem Rev* **2013**, *113*, 6621.
(8) Cheng, D. J.; Negreiros, F. R.; Apra, E.; Fortunelli, A. *Chemsuschem* **2013**, *6*, 944.
(9) Li, Y. W.; Chan, S. H.; Sun, Q. *Nanoscale* **2015**, *7*, 8663.
(10) Kondratenko, E. V.; Mul, G.; Baltrusaitis, J.; Larrazabal, G. O.; Perez-Ramirez, J. *Energ Environ Sci* **2013**, *6*, 3112.
(11) Saeidi, S.; Amin, N. A. S.; Rahimpour, M. R. *J Co2 Util* **2014**, *5*, 66.
(12) Aresta, M.; Dibenedetto, A.; Angelini, A. *J Co2 Util* **2013**, *3-4*, 65.
(13) Hu, B.; Guild, C.; Suib, S. L. *J Co2 Util* **2013**, *1*, 18.
(14) Lahijani, P.; Zainal, Z. A.; Mohammadi, M.; Mohamed, A. R. *Renew Sust Energ Rev* **2015**, *41*, 615.
(15) Porosoff, M. D.; Yan, B. H.; Chen, J. G. G. *Energ Environ Sci* **2016**, *9*, 62.
(16) Qiao, J. L.; Liu, Y. Y.; Hong, F.; Zhang, J. J. *Chem Soc Rev* **2014**, *43*, 631.
(17) Kuhl, K. P.; Cave, E. R.; Abram, D. N.; Jaramillo, T. F. *Energ Environ Sci* **2012**, *5*, 7050.
(18) Kuhl, K. P.; Hatsukade, T.; Cave, E. R.; Abram, D. N.; Kibsgaard, J.; Jaramillo, T. F. *J Am Chem Soc* **2014**, *136*, 14107.
(19) Zhu, W. L.; Zhang, Y. J.; Zhang, H. Y.; Lv, H. F.; Li, Q.; Michalsky, R.; Peterson, A. A.; Sun, S. H. *J Am Chem Soc* **2014**, *136*, 16132.
(20) Torelli, D. A.; Francis, S. A.; Crompton, J. C.; Javier, A.; Thompson, J. R.; Brunschwig, B. S.; Soriaga, M. P.; Lewis, N. S. *Acs Catal* **2016**, *6*, 2100.
(21) Hahn, C.; Abram, D. N.; Hansen, H. A.; Hatsukade, T.; Jackson, A.; Johnson, N. C.; Hellstern, T. R.; Kuhl, K. P.; Cave, E. R.; Feaster, J. T.; Jaramillo, T. F. *J Mater Chem A* **2015**, *3*, 20185.

(22) Peterson, A. A.; Abild-Pedersen, F.; Studt, F.; Rossmeisl, J.; Norskov, J. K. *Energy Environ. Sci.* **2010**, *3*, 1311.
(23) Schouten, K. J. P.; Gallent, E. P.; Koper, M. T. M. *Acs Catal* **2013**, *3*, 1292.
(24) Calle-Vallejo, F.; Koper, M. T. M. *Angew Chem Int Edit* **2013**, *52*, 7282.
(25) Reske, R.; Duca, M.; Oezaslan, M.; Schouten, K. J. P.; Koper, M. T. M.; Strassert, P. *J Phys Chem Lett* **2013**, *4*, 2410.
(26) Kortlever, R.; Shen, J.; Schouten, K. J. P.; Calle-Vallejo, F.; Koper, M. T. M. *J Phys Chem Lett* **2015**, *6*, 4073.
(27) Lu, Q.; Rosen, J.; Zhou, Y.; Hutchings, G. S.; Kimmel, Y. C.; Chen, J. G. G.; Jiao, F. *Nat Commun* **2014**, *5*.
(28) Graciani, J.; Mudiyanselage, K.; Xu, F.; Baber, A. E.; Evans, J.; Senanayake, S. D.; Stacchiola, D. J.; Liu, P.; Hrbek, J.; Sanz, J. F.; Rodriguez, J. A. *Science* **2014**, *345*, 546.
(29) Kuld, S.; Thorhauge, M.; Falsig, H.; Elkjaer, C. F.; Helveg, S.; Chorkendorff, I.; Sehested, J. *Science* **2016**, *352*, 969.
(30) Behrens, M.; Studt, F.; Kasatkin, I.; Kuhl, S.; Havecker, M.; Abild-Pedersen, F.; Zander, S.; Girgsdies, F.; Kurr, P.; Kniep, B. L.; Tovar, M.; Fischer, R. W.; Norskov, J. K.; Schlogl, R. *Science* **2012**, *336*, 893.
(31) Hartadi, Y.; Widmann, D.; Behm, R. J. *Chemsuschem* **2015**, *8*, 456.
(32) Dorner, R. W.; Hardy, D. R.; Williams, F. W.; Willauer, H. D. *Energ Environ Sci* **2010**, *3*, 884.
(33) Rodriguez, J. A.; Liu, P.; Stacchiola, D. J.; Senanayake, S. D.; White, M. G.; Chen, J. G. G. *Acs Catal* **2015**, *5*, 6696.
(34) Damen, K.; van Troost, M.; Faaij, A.; Turkenburg, W. *Prog Energ Combust* **2006**, *32*, 215.
(35) Goeppert, A.; Czaun, M.; Jones, J. P.; Prakash, G. K. S.; Olah, G. A. *Chem Soc Rev* **2014**, *43*, 7995.
(36) Daza, Y. A.; Kuhn, J. N. *Rsc Adv* **2016**, *6*, 49675.
(37) Yang, X. F.; Kattel, S.; Senanayake, S. D.; Boscoboinik, J. A.; Nie, X. W.; Graciani, J.; Rodriguez, J. A.; Liu, P.; Stacchiola, D. J.; Chen, J. G. G. *J Am Chem Soc* **2015**, *137*, 10104.
(38) Kattel, S.; Yan, B. H.; Yang, Y. X.; Chen, J. G. G.; Liu, P. *J Am Chem Soc* **2016**, *138*, 12440.
(39) Kattel, S.; Yu, W. T.; Yang, X. F.; Yan, B. H.; Huang, Y. Q.; Wan, W. M.; Liu, P.; Chen, J. G. G. *Angew Chem Int Edit* **2016**, *55*, 7968.
(40) Senanayake, S. D.; Ramirez, P. J.; Waluyo, I.; Kundu, S.; Mudiyanselage, K.; Liu, Z. Y.; Liu, Z.; Axnanda, S.; Stacchiola, D. J.; Evans, J.; Rodriguez, J. A. *J Phys Chem C* **2016**, *120*, 1778.
(41) Zhou, X. W.; Qu, J.; Xu, F.; Hu, J. P.; Foord, J. S.; Zeng, Z. Y.; Hong, X. L.; Tsang, S. C. E. *Chem Commun* **2013**, *49*, 1747.
(42) Li, D.; Ichikuni, N.; Shimazu, S.; Uematsu, T. *Appl Catal a-Gen* **1999**, *180*, 227.
(43) Kim, C. H.; Lee, J. S.; Trimm, D. L. *Carbon Dioxide Utilization for Global Sustainability* **2004**, *153*, 61.
(44) Wang, J.; Funk, S.; Burghaus, U. *Catal Lett* **2005**, *103*, 219.
(45) Hicks, R. F.; Bell, A. T. *J Catal* **1984**, *90*, 205.
(46) Trovarelli, A.; Dolcetti, G.; Deleitenburg, C.; Kaspar, J. *Studies in Surface Science and Catalysis* **1993**, *75*, 2781.
(47) Kattel, S.; Ramirez, P. J.; Chen, J. G.; Rodriguez, J. A.; Liu, P. *Science* **2017**, *355*, 1296.
(48) Tang, Q. L.; Hong, Q. J.; Liu, Z. P. *J Catal* **2009**, *263*, 114.
(49) Larmier, K.; Liao, W. C.; Tada, S.; Lam, E.; Verel, R.; Bansode, A.; Urakawa, A.; Comas-Vives, A.; Coperet, C. *Angew Chem Int Edit* **2017**, *56*, 2318.
(50) Mehta, P.; Greeley, J.; Delgass, W. N.; Schneider, W. F.,. Acs Catal 2017, 4707-4715.
(51) Kattel, S.; Yan, B. H.; Chen, J. G. G.; Liu, P. *J Catal* **2016**, *343*, 115.
(52) Kim, S. S.; Lee, H. H.; Hong, S. C. *Appl Catal B-Environ* **2012**, *119*, 100.

(53) Goguet, A.; Shekhtman, S. O.; Burch, R.; Hardacre, C.; Meunier, E.; Yablonsky, G. S. *J Catal* **2006**, *237*, 102.
(54) Goguet, A.; Meunier, F.; Breen, J. P.; Burch, R.; Petch, M. I.; Ghenciu, A. F. *J Catal* **2004**, *226*, 382.
(55) Kim, S. S.; Lee, H. H.; Hong, S. C. *Appl Catal a-Gen* **2012**, *423*, 100.
(56) Pettigrew, D. J.; Trimm, D. L.; Cant, N. W. *Catal Lett* **1994**, *28*, 313.
(57) Inoue, T.; Iizuka, T.; Tanabe, K. *Appl Catal* **1989**, *46*, 1.
(58) Ishito, N.; Hara, K.; Nakajima, K.; Fukuoka, A. *J Energy Chem* **2016**, *25*, 306.
(59) Wang, L. C.; Khazaneh, M. T.; Widmann, D.; Behm, R. J. *J Catal* **2013**, *302*, 20.
(60) Wang, G. C.; Nakamura, J. *J Phys Chem Lett* **2010**, *1*, 3053.
(61) Chen, C. S.; Cheng, W. H.; Lin, S. S. *Chem Commun* **2001**, 1770.
(62) Chen, C. S.; Cheng, W. H. *Catal Lett* **2002**, *83*, 121.
(63) Chen, C. S.; Cheng, W. H.; Lin, S. S. *Catal Lett* **2000**, *68*, 45.
(64) Yoshihara, J.; Parker, S. C.; Schafer, A.; Campbell, C. T. *Catal Lett* **1995**, *31*, 313.
(65) Nakamura, I.; Fujitani, T.; Uchijima, T.; Nakamura, J. *Surf Sci* **1998**, *400*, 387.
(66) Wang, G. C.; Jiang, L.; Pang, X. Y.; Cai, Z. S.; Pan, Y. M.; Zhao, X. Z.; Morikawa, Y.; Nakamura, J. *Surf Sci* **2003**, *543*, 118.
(67) Loiland, J. A.; Wulfers, M. J.; Marinkovic, N. S.; Lobo, R. F. *Catal Sci Technol* **2016**, *6*, 5267.
(68) Wolf, A.; Jess, A.; Kern, C. *Chem Eng Technol* **2016**, *39*, 1040.
(69) Wang, L. H.; Liu, H.; Liu, Y.; Chen, Y.; Yang, S. Q. *J Rare Earth* **2013**, *31*, 969.
(70) Wang, L. H.; Liu, Y. *Abstr Pap Am Chem S* **2006**, *232*.
(71) Sun, F. M.; Yan, C. F.; Wang, Z. D.; Guo, C. Q.; Huang, S. L. *Int J Hydrogen Energ* **2015**, *40*, 15985.
(72) Fujita, S.; Usui, M.; Takezawa, N. *J Catal* **1992**, *134*, 220.
(73) Porosoff, M. D.; Chen, J. G. G. *J Catal* **2013**, *301*, 30.
(74) Kusama, H.; Bando, K. K.; Okabe, K.; Arakawa, H. *Appl Catal a-Gen* **2001**, *205*, 285.
(75) Matsubu, J. C.; Yang, V. N.; Christopher, P. *J Am Chem Soc* **2015**, *137*, 3076.
(76) Porosoff, M. D.; Yang, X. F.; Boscoboinik, J. A.; Chen, J. G. G. *Angew Chem Int Edit* **2014**, *53*, 6705.
(77) Ye, J. Y.; Liu, C. J.; Mei, D. H.; Ge, Q. F. *J Catal* **2014**, *317*, 44.
(78) Yang, B.; Liu, C.; Halder, A.; Tyo, E. C.; Martinson, A. B. F.; Seifer, S.; Zapol, P.; Curtiss, L. A.; Vajda, S. *J Phys Chem C* **2017**, *121*, 10406.
(79) Zhang, R. G.; Wang, B. J.; Liu, H. Y.; Ling, L. X. *J Phys Chem C* **2011**, *115*, 19811.
(80) Pan, Y. X.; Liu, C. J.; Ge, Q. F. *J Catal* **2010**, *272*, 227.
(81) Rozanov, V. V.; Krylov, O. V. *Usp Khim+* **1997**, *66*, 117.
(82) Conner, W. C.; Falconer, J. L. *Chem Rev* **1995**, *95*, 759.
(83) Ye, J. Y.; Liu, C. J.; Mei, D. H.; Ge, Q. F. *Acs Catal* **2013**, *3*, 1296.
(84) Cheng, Z.; Sherman, B. J.; Lo, C. S. *J Chem Phys* **2013**, *138*.
(85) Huygh, S.; Bogaerts, A.; Neyts, E. C. *J Phys Chem C* **2016**, *120*, 21659.
(86) Pan, Y. X.; Liu, C. J.; Mei, D. H.; Ge, Q. F. *Langmuir* **2010**, *26*, 5551.
(87) Strunk, J.; Kaehler, K.; Xia, X. Y.; Comotti, M.; Schuth, F.; Reinecke, T.; Muhler, M. *Appl Catal a-Gen* **2009**, *359*, 121.
(88) Iizuka, T.; Kojima, M.; Tanabe, K. *J Chem Soc Chem Comm* **1983**, 638.
(89) Man, I. C.; Su, H. Y.; Calle-Vallejo, F.; Hansen, H. A.; Martinez, J. I.; Inoglu, N. G.; Kitchin, J.; Jaramillo, T. F.; Norskov, J. K.; Rossmeisl, J. *Chemcatchem* **2011**, *3*, 1159.
(90) Yang, Y.; White, M. G.; Liu, P. *The Journal of Physical Chemistry C* **2012**, *116*, 248.
(91) Martin, O.; Mondelli, C.; Cervellino, A.; Ferri, D.; Curulla-Ferre, D.; Perez-Ramirez, J. *Angew Chem Int Edit* **2016**, *55*, 11031.
(92) Martin, O.; Martin, A. J.; Mondelli, C.; Mitchell, S.; Segawa, T. F.; Hauert, R.; Drouilly, C.; Curulla-Ferre, D.; Perez-Ramirez, J. *Angew Chem Int Edit* **2016**, *55*, 6261.

(93) Park, J. N.; McFarland, E. W. *J Catal* **2009**, *266*, 92.
(94) Fujitani, T.; Saito, M.; Kanai, Y.; Watanabe, T.; Nakamura, J.; Uchijima, T. *Appl Catal a-Gen* **1995**, *125*, L199.
(95) Fan, L.; Fujimoto, K. *J Catal* **1997**, *172*, 238.
(96) Collins, S. E.; Chiavassa, D. L.; Bonivardi, A. L.; Baltanas, M. A. *Catal Lett* **2005**, *103*, 83.
(97) Qu, J.; Zhou, X. W.; Xu, F.; Gong, X. Q.; Tsang, S. C. E. *J Phys Chem C* **2014**, *118*, 24452.
(98) Tsubaki, N.; Fujimoto, K. *Top Catal* **2003**, *22*, 325.
(99) Bahruji, H.; Bowker, M.; Hutchings, G.; Dimitratos, N.; Wells, P.; Gibson, E.; Jones, W.; Brookes, C.; Morgan, D.; Lalev, G. *J Catal* **2016**, *343*, 133.
(100) Sakurai, H.; Haruta, M. *Catal Today* **1996**, *29*, 361.
(101) Lunkenbein, T.; Schumann, J.; Behrens, M.; Schlogl, R.; Willinger, M. G. *Angew Chem Int Edit* **2015**, *54*, 4544.
(102) van den Berg, R.; Prieto, G.; Korpershoek, G.; van der Wal, L. I.; van Bunningen, A. J.; Laegsgaard-Jorgensen, S.; de Jongh, P. E.; de Jong, K. P. *Nat Commun* **2016**, *7*.
(103) Lunkenbein, T.; Girgsdies, F.; Kandemir, T.; Thomas, N.; Behrens, M.; Schlogl, R.; Frei, E. *Angew Chem Int Edit* **2016**, *55*, 12708.
(104) Hartadi, Y.; Widmann, D.; Behm, R. J. *J Catal* **2016**, *333*, 238.
(105) Tisseraud, C.; Comminges, C.; Belin, T.; Ahouari, H.; Soualah, A.; Pouilloux, Y.; Le Valant, A. *J Catal* **2015**, *330*, 533.
(106) Tisseraud, C.; Comminges, C.; Pronier, S.; Pouilloux, Y.; Le Valant, A. *J Catal* **2016**, *343*, 106.
(107) Le Valant, A.; Comminges, C.; Tisseraud, C.; Canaff, C.; Pinard, L.; Pouilloux, Y. *J Catal* **2015**, *324*, 41.
(108) Erdohelyi, A.; Pasztor, M.; Solymosi, F. *J Catal* **1986**, *98*, 166.
(109) Kim, C. H.; Lee, J. S.; Trimm, D. L. *Top Catal* **2003**, *22*, 319.
(110) Fan, L.; Fujimoto, K. *Appl Catal a-Gen* **1993**, *106*, L1.
(111) Fan, L.; Fujimoto, K. *J Catal* **1994**, *150*, 217.
(112) Sakurai, H.; Tsubota, S.; Haruta, M. *Appl Catal a-Gen* **1993**, *102*, 125.
(113) Grabow, L. C.; Mavrikakis, M. *Acs Catal* **2011**, *1*, 365.
(114) Studt, F.; Behrens, M.; Kunkes, E. L.; Thomas, N.; Zander, S.; Tarasov, A.; Schumann, J.; Frei, E.; Varley, J. B.; Abild-Pedersen, F.; Norskov, J. K.; Schlogl, R. *Chemcatchem* **2015**, *7*, 1105.
(115) Studt, F.; Sharafutdinov, I.; Abild-Pedersen, F.; Elkjaer, C. F.; Hummelshoj, J. S.; Dahl, S.; Chorkendorff, I.; Norskov, J. K. *Nat Chem* **2014**, *6*, 320.
(116) Zhao, Y. F.; Yang, Y.; Mims, C.; Peden, C. H. F.; Li, J.; Mei, D. H. *J Catal* **2011**, *281*, 199.
(117) Liu, C.; Yang, B.; Tyo, E.; Seifert, S.; DeBartolo, J.; von Issendorff, B.; Zapol, P.; Vajda, S.; Curtiss, L. A. *J Am Chem Soc* **2015**, *137*, 8676.
(118) Aziz, M. A. A.; Jalil, A. A.; Triwahyono, S.; Mukti, R. R.; Taufiq-Yap, Y. H.; Sazegar, M. R. *Appl Catal B-Environ* **2014**, *147*, 359.
(119) Wu, H. C.; Chang, Y. C.; Wu, J. H.; Lin, J. H.; Lin, I. K.; Chen, C. S. *Catal Sci Technol* **2015**, *5*, 4154.
(120) Rahmani, S.; Rezaei, M.; Meshkani, F. *J Ind Eng Chem* **2014**, *20*, 1346.
(121) Lim, J. Y.; McGregor, J.; Sederman, A. J.; Dennis, J. S. *Chem Eng Sci* **2016**, *141*, 28.
(122) Lim, J. Y.; McGregor, J.; Sederman, A. J.; Dennis, J. S. *Chem Eng Sci* **2016**, *152*, 754.
(123) Danaci, S.; Protasova, L.; Lefevere, J.; Bedel, L.; Guilet, R.; Marty, P. *Catal Today* **2016**, *273*, 234.
(124) Akamaru, S.; Shimazaki, T.; Kubo, M.; Abe, T. *Appl Catal a-Gen* **2014**, *470*, 405.
(125) Tada, S.; Shimizu, T.; Kameyama, H.; Haneda, T.; Kikuchi, R. *Int J Hydrogen Energ* **2012**, *37*, 5527.

(126) Zhou, G. L.; Liu, H. R.; Cui, K. K.; Jia, A. P.; Hu, G. S.; Jiao, Z. J.; Liu, Y. Q.; Zhang, X. M. *Appl Surf Sci* **2016**, *383*, 248.

(127) Aldana, P. A. U.; Ocampo, F.; Kobl, K.; Louis, B.; Thibault-Starzyk, F.; Daturi, M.; Bazin, P.; Thomas, S.; Roger, A. C. *Catal Today* **2013**, *215*, 201.

(128) da Silva, D. C. D.; Letichevsky, S.; Borges, L. E. P.; Appel, L. G. *Int J Hydrogen Energ* **2012**, *37*, 8923.

(129) Ocampo, F.; Louis, B.; Kiwi-Minsker, L.; Roger, A. C. *Appl Catal a-Gen* **2011**, *392*, 36.

(130) Tada, S.; Ochieng, O. J.; Kikuchi, R.; Haneda, T.; Kameyama, H. *Int J Hydrogen Energ* **2014**, *39*, 10090.

(131) Sharma, S.; Hu, Z. P.; Zhang, P.; McFarland, E. W.; Metiu, H. *J Catal* **2011**, *278*, 297.

(132) Sharma, S.; Kumar, K. B. S.; Chandnani, Y. M.; Kumar, V. S. P.; Gangwar, B. P.; Singhal, A.; Deshpande, P. A. *J Phys Chem C* **2016**, *120*, 14101.

(133) Abdel-Mageed, A. M.; Eckle, S.; Widmann, D.; Behm, R. J. *J Catal* **2016**, *335*, 79.

(134) Eckle, S.; Augustin, M.; Anfang, H. G.; Behm, R. J. *Catal Today* **2012**, *181*, 40.

(135) Janke, C.; Duyar, M. S.; Hoskins, M.; Farrauto, R. *Appl Catal B-Environ* **2014**, *152*, 184.

(136) Duyar, M. S.; Ramachandran, A.; Wang, C.; Farrauto, R. J. *J Co2 Util* **2015**, *12*, 27.

(137) Abe, T.; Tanizawa, M.; Watanabe, K.; Taguchi, A. *Energ Environ Sci* **2009**, *2*, 315.

(138) Upham, D. C.; Derk, A. R.; Sharma, S.; Metiu, H.; McFarland, E. W. *Catal Sci Technol* **2015**, *5*, 1783.

(139) Zhang, S. T.; Yan, H.; Wei, M.; Evans, D. G.; Duan, X. *Rsc Adv* **2014**, *4*, 30241.

(140) Wang, F.; He, S.; Chen, H.; Wang, B.; Zheng, L. R.; Wei, M.; Evans, D. G.; Duan, X. *J Am Chem Soc* **2016**, *138*, 6298.

(141) Beuls, A.; Swalus, C.; Jacquemin, M.; Heyen, G.; Karelovic, A.; Ruiz, P. *Appl Catal B-Environ* **2012**, *113*, 2.

(142) Xu, J. H.; Su, X.; Duan, H. M.; Hou, B. L.; Lin, Q. Q.; Liu, X. Y.; Pan, X. L.; Pei, G. X.; Geng, H. R.; Huang, Y. Q.; Zhang, T. *J Catal* **2016**, *333*, 227.

(143) Ren, J.; Guo, H. L.; Yang, J. Z.; Qin, Z. F.; Lin, J. Y.; Li, Z. *Appl Surf Sci* **2015**, *351*, 504.

(144) Miao, B.; Ma, S. S. K.; Wang, X.; Su, H. B.; Chan, S. H. *Catal Sci Technol* **2016**, *6*, 4048.

(145) Bothra, P.; Periyasamy, G.; Pati, S. K. *Phys Chem Chem Phys* **2013**, *15*, 5701.

(146) Avanesian, T.; Gusmao, G. S.; Christopher, P. *J Catal* **2016**, *343*, 86.

(147) Razzaq, R.; Zhu, H. W.; Jiang, L.; Muhammad, U.; Li, C. S.; Zhang, S. J. *Ind Eng Chem Res* **2013**, *52*, 2247.

(148) Shashidhara, G. M.; Ravindram, M. *React Kinet Catal L* **1988**, *37*, 451.

(149) Yang, Y. X.; Evans, J.; Rodriguez, J. A.; White, M. G.; Liu, P. *Phys Chem Chem Phys* **2010**, *12*, 9909.

(150) Yang, Y.; Mims, C. A.; Mei, D. H.; Peden, C. H. F.; Campbell, C. T. *J Catal* **2013**, *298*, 10.

(151) Avanesian, T.; Christopher, P. *Acs Catal* **2016**, *6*, 5268.

(152) Norskov, J. K.; Rossmeisl, J.; Logadottir, A.; Lindqvist, L.; Kitchin, J. R.; Bligaard, T.; Jonsson, H. *J Phys Chem B* **2004**, *108*, 17886.

(153) Greeley, J.; Stephens, I. E. L.; Bondarenko, A. S.; Johansson, T. P.; Hansen, H. A.; Jaramillo, T. F.; Rossmeisl, J.; Chorkendorff, I.; Norskov, J. K. *Nat Chem* **2009**, *1*, 552.

(154) Rossmeisl, J.; Qu, Z. W.; Zhu, H.; Kroes, G. J.; Norskov, J. K. *J Electroanal Chem* **2007**, *607*, 83.

(155) Karelovic, A.; Ruiz, P. *Appl Catal B-Environ* **2012**, *113*, 237.

(156) Melaet, G.; Lindeman, A. E.; Somorjai, G. A. *Top Catal* **2014**, *57*, 500.

(157) Matsubu, J. C.; Zhang, S. Y.; DeRita, L.; Marinkovic, N. S.; Chen, J. G. G.; Graham, G. W.; Pan, X. Q.; Christopher, P. *Nat Chem* **2017**, *9*, 120.

(158) Koeppel, R. A.; Baiker, A.; Wokaun, A. *Appl Catal a-Gen* **1992**, *84*, 77.

(159) Kilo, M.; Weigel, J.; Wokaun, A.; Koeppel, R. A.; Stoeckli, A.; Baiker, A. *J Mol Catal a-Chem* **1997**, *126*, 169.

(160) Wang, J. B.; Lee, H. K.; Huang, T. J. *Catal Lett* **2002**, *83*, 79.
(161) Lei, H.; Nie, R. F.; Wu, G. Q.; Hou, Z. Y. *Fuel* **2015**, *154*, 161.
(162) Li, C.; Yuan, X.; Fujimoto, K. *Appl Catal a-Gen* **2014**, *469*, 306.
(163) Liu, Y.; Zhang, Y.; Wang, T. J.; Tsubaki, N. *Chem Lett* **2007**, *36*, 1182.
(164) Sloczynski, J.; Grabowski, R.; Kozlowska, A.; Olszewski, P.; Stoch, J.; Skrzypek, J.; Lachowska, M. *Appl Catal a-Gen* **2004**, *278*, 11.
(165) Lachowska, M.; Skrzypek, J. *React Kinet Catal L* **2004**, *83*, 269.
(166) Liao, F. L.; Huang, Y. Q.; Ge, J. W.; Zheng, W. R.; Tedsree, K.; Collier, P.; Hong, X. L.; Tsang, S. C. *Angew Chem Int Edit* **2011**, *50*, 2162.
(167) Collins, S. E.; Baltanas, M. A.; Bonivardi, A. L. *J Catal* **2004**, *226*, 410.
(168) Gogate, M. R.; Davis, R. J. *Catal Commun* **2010**, *11*, 901.
(169) Kharaji, A. G.; Shariati, A.; Ostadi, M. *J Nanosci Nanotechno* **2014**, *14*, 6841.
(170) Liu, Y.; Liu, D. Z. *Int J Hydrogen Energ* **1999**, *24*, 351.
(171) Kharaji, A. G.; Shariati, A.; Takassi, M. A. *Chinese J Chem Eng* **2013**, *21*, 1007.
(172) Razzaq, R.; Li, C. S.; Usman, M.; Suzuki, K.; Zhang, S. J. *Chem Eng J* **2015**, *262*, 1090.

Table 1. Summary of reaction conditions with CO_2 conversion and selectivity on metal/oxide catalysts.

Catalyst	H_2:CO_2 ratio	Temperature (^{0}C)	Pressure (MPa)	Conversion (%)	Selectivity (%)		
					CO	CH_3OH	CH_4
Cu/TiO_2[38]	3:1	220	0.1	0.54	83.6	13.8	
Cu/ZrO_2[38]	3:1	220	0.1	0.53	80.2	19.8	
Cu/ZrO_2[158]	3:1	220	1.7	6		67	
Cu/ZrO_2[159]	3:1	350	1.7	6.9		70	
Cu/Al_2O_3[160]	5:1	250	3	N/A	44.54	54.91	0.55
$Cu/CeO_2/\gamma$-Al_2O_3[160]	5:1	250	3	N/A	27.97	71.94	0.09
Cu/YDC//γ-Al_2O_3[160]	5:1	250	3	N/A	21.28	78.69	0.03
$Cu/MnO_x/ZrO_2$[159]	3:1	350	1.7	4.8		58	
$Cu/CrO_x/ZrO_2$[159]	3:1	350	1.7	4		87	
Cu/ZnO[94]	3:1	250	5	11.7	63.9	36.1	0
Cu/ZnO-rod[161]	3:1	240	3	8		61.8	
Cu/ZnO-filament[161]	3:1	240	3	16.5		78.2	
$Cu/ZnO/Al_2O_3$[162]	3:1	230	3	18.7		43	
Cu/ZnO[163]	2.8:1	170	5	5.2	85.4	11.9	
$Cu/ZnO/Al_2O_3$[163]	2.8:1	170	5	14.3	45.1	54.8	
$Cu/ZnO/ZrO_2/Al_2O_3$[162]	3:1	230	3	23.2		60.3	
$Cu/ZnO/ZrO_2$[162]	3:1	230	3	19.3		48.6	
$Cu/ZnO/ZrO_2$[164]	3:1	220	8	21		68	
$Cu/Zn/ZrO_2$-Mn-promoted[165]	3:1	280	10	16		91	
Cu/rod ZnO/Al_2O_3[166]	2.2:1	270	4.5	12.3		42.3	
Cu/plate ZnO/Al_2O_3[166]	2.2:1	270	4.5	10.9		72.7	
Pd/CeO_2[110]	3:1	200	3	2.1	6.3	92.9	0.8
Pd/CeO_2[110]	3:1	220	3	2.5	7.1	92.1	0.8
Pd/CeO_2[110]	3:1	230	3	3.1	7.1	91.7	1.1
Pd/CeO_2[110]	3:1	240	3	4.4	11.2	85.2	3.5
Pd/CeO_2[110]	3:1	260	3	5.2	11	84.7	4.3
Pd/Al_2O_3[94]	3:1	250	5	3.4	51.5	29.9	18.6
Pd/Cr_2O_3[94]	3:1	250	5	2.1	65	22.4	12.6
Pd/β-Ga_2O_3[167]	3:1	250	3	0.86	48	52	0
Pd/Ga_2O_3[94]	3:1	250	5	19.6	47.9	51.5	0.5
Pd/rod Ga_2O_3[41]	3:1	250	5	11		41.3	

Pd/plate Ga_2O_3[41]	3:1	250	5	17.3		51.6	
Pd/SiO_2[94]	3:1	250	5	0.05	0	100	0
Pd/TiO_2[94]	3:1	250	5	15.5	95.9	3.9	0.2
Pd/ZnO[94]	3:1	250	5	13.8	62.3	37.5	0.1
Pd/ZnO (1% Pd), SI[99]; SI = sol immobilization,	3:1	250	2	1.7	24	76	
Pd/ZnO (1% Pd), IM[99]; IM = impregnation	3:1	250	2	3.2	78	22	
Pd/ZnO (5% Pd), SI	3:1	250	2	10.7	39	60	
Pd/ZnO (5% Pd), IM	3:1	250	2	8.7	99	1	
Pd/ZrO_2[94]	3:1	250	5	0.4	81.7	4.3	14
Pd/Al_2O_3[108]	4:1	275	0.95	1.2		5.4	
Pd/Al_2O_3[108]	2:1	275	0.95	0.23		49.1	
Pd/TiO_2[108]	4:1	275	0.95	3.9		1.98	
Pd/SiO_2[108]	4:1	275	0.95	0.8		9.5	
Pd/SiO_2[108]	2:1	275	0.95	0.7		89.0	
Pd/MgO[108]	4:1	275	0.95	0.77		7.8	
Pd/MgO[108]	2:1	275	0.95	0.65		96.5	
Pd/Al_2O_3-fresh[56]	1:1	240	0.1	30			22
Pd/Al_2O_3-aged[56]	1:1	240	0.1	30			39
Pd/La_2O_3/Al_2O_3[56]	1:1	240	0.1	30			30
Pd/PrO_2/Al_2O_3[56]	1:1	240	0.1	30			24
Pd/CeO_2(5)/Al_2O_3[56]	1:1	240	0.1	30			13
Pd/CeO_2(10)/Al_2O_3[56]	1:1	240	0.1	30			19
Pd/SiO_2[93]	4:1	450	0.1	40.8	89.6		10.4
Au/ZrO_2[31]	3:1	220	0.5	5.3		5	
Au/ZrO_2[31]	3:1	240	0.5	9.3		3.4	
Au/ZnO[31]	3:1	220	0.5	0.2		56.2	
Au/ZnO[31]	3:1	240	0.5	0.4		50.6	
Au/ZnO/ZrO_2[164]	3:1	220	8	1.5		100	
Au/Al_2O_3[31]	3:1	220	0.5	2		1.5	
Au/Al_2O_3[31]	3:1	240	0.5	3.7		0.4	
Pt/SiO_2[51]	2:1	553	0.1	2.03	100		0
Pt/TiO_2[51]	2:1	553	0.1	2.99	99.22		0.78
Ni/SiO_2[93]	4:1	450	0.1	36.8	18.2		81.8
Ni/γ-Al_2O_3[120]	3.5	350	0.1	~75			100

Ni/Al_2O_3[123]	4:1	250	0.1	39			97
Ni/SiO_2[127]	4:1	350	0.1	27.6	11.6		85.5
Ni/SiO_2[118]	4:1	300	0.1	42.4	3.4		96.6
$0.5\%Ni/SiO_2$[119]	N/A	350	0.1	~10	~40		~60
$10\%Ni/SiO_2$[119]	N/A	350	0.1	~10	~10		~90
Ni/CeO_2[125]	5:1	450	0.1	~80			~100
Ni/CeO_2[126]	4.6	340	0.1	91.1			100
Ni/ZrO_2[128]	12.5	377	0.1	~100			**~100**
$Ni/Ce_xZr_{1-x}O_2$[129]	4:1	350	0.1	71.5	0.9		98.5
$Ni/CeO_2/ZrO_2$-sol-gel[127]	4:1	350	0.1	67.9	1.4		98.4
$Ni/CeO_2/ZrO_2$-imp[127]	4:1	350	0.1	25.4	14.5		84.7
Re/ZrO_2[88]	N/A	160	1	N/A		73.2	25.5
Re/Nb_2O_5[88]	N/A	220	1	N/A		52.0	37.6
Re/MgO[88]	N/A	260	1	N/A		17.5	80.6
Re/SiO_2[88]	N/A	180	1	N/A		22.6	74.7
Re/Zeolon[88]	N/A	220	1	N/A		18.2	75.7
$Rh/\gamma\text{-}Al_2O_3$[141]	4:1	200	0.1	~98			~100
Rh/SiO_2[74]	3:1	200	5	0.52	88.1	6.8	5.1
Rh/TiO_2[168]	1:1	270	2	7.89	14.5	0.80	72.7
Rh/TiO_2[57]	3:1	240	1	N/A		60.7	32.4
Rh/ZrO_2[57]	3:1	240	1	N/A			99.9
Rh/MgO[57]	3:1	240	1	N/A		1	99
Rh/Nb_2O_5[57]	3:1	260	1	N/A			100
Ru/TiO_2[137]	4:1	160	0.1	N/A			100
$Ru_{0.01}Ce_{0.99}O_2$[131]	4:1	500	N/A	16			90
Ru/CeO_2[140]	4:1	250	0.1	92.7			
Ru/Al_2O_3[133]	~5:1	190	0.1	N/A			42
$Ru/CeO_2/Al_2O_3$[130]	4:1	250	0.1	~20			~100
$Ag/ZnO/ZrO_2$[164]	3:1	220	8	2		97	
Co/CeO_2[76]	3:1	300	0.1	3.8	39.4		
$Co/\gamma\text{-}Al_2O_3$[76]	3:1	300	0.1	3.8	67.0		
Fe/TiO_2[168]	1:1	270	2	2.65	73	0.0	11.6
Mg/SiO_2[93]	4:1	450	0.1	0.8	89.7		10.3
$Mo/\gamma\text{-}Al_2O_3$[169]	1:1	600	1	34.2	97		
$Cu\text{-}Ni/\gamma\text{-}Al_2O_3$[170]	1:1	600	0.1	28.7	79.7		20.3
$Pd\text{-}Fe/SiO_2$[93]	4:1	450	0.1	44.7	97.2		2.8

Pd-Mg/SiO_2[93]	4:1	450	0.1	59.2	4.7		95.3
Pd-Li/SiO_2[93]	4:1	450	0.1	42.6	11.5		88.5
Pd-Ni/SiO_2[93]	4:1	450	0.1	50.5	11.0		89
PtCo/CeO_2[76]	3:1	300	0.1	3.3	71		
PtCo/γ-Al_2O_3[76]	3:1	300	0.1	5.1	89.4		
PtCo/TiO_2[39]	2:1	300	0.1	8.2	~99		~1
PtCo/CeO_2[39]	2:1	300	0.1	9.1	~92		~8
PtCo/ZrO_2[39]	2:1	300	0.1	7.8	~89		~11
15Ni-5Co/Al_2O_3-CeO_2[147]	~19	300	2	N/A			100
15Ni-5Co/$Zr_{0.75}Ce_{0.25}O_2$[147]	~19	300	2	N/A			99
15Ni-5Co/Al_2O_3-ZrO_2[147]	~19	300	2	N/A			98
Fe-Mo/γ-Al_2O_3[171]	1:1	600	1	~45	~100		
Rh-Fe/TiO_2[168]	1:1	270	2	9.16	28.4	1.26	57.2
Co_4N/γ-Al_2O_3[172]	~19	300	1.5	~98			~98

Table 2. First-order consumption rate constants for CO_2 conversion by H_2 normalized by catalyst weight and CO uptake values. For bimetallic catalysts, the metal loading corresponds to a Ni/Pt (Co/Pt or Ni/Pd) atomic ratio of 3 to 1. Reproduced with permission from ref [73]. Copyright 2013 Elsevier.

Catalysts	Metal loading (wt%)	CO uptake (μ mol g^{-1} cat)	k_r (10^{-3} min^{-1} g^{-1} cat)	Normalized k_r (10^{-3} min^{-1} mol CO^{-1})	CO/CH_4 ratio at 10% conversion
$PtNi/CeO_2$	1.7% Pt, 1.5% Ni	35.4	11.43	0.323	60.7
Pt/CeO_2	1.7% Pt	14.1	2.88	0.204	150.7
Ni/CeO_2	1.5% Ni	11.2	9.26	0.827	27.5
$PdNi/CeO_2$	0.91% Pd, 1.5% Ni	36.0	12.51	0.347	31.9
$PtCo/CeO_2$	1.7% Pt, 1.5% Co	37.2	6.29	0.169	259.4
Co/CeO_2	1.5% Co	4.0	3.56	0.889	43.0
$PtNi/\gamma\text{-}Al_2O_3$	1.7% Pt, 1.5% Ni	44.4	4.18	0.094	62.1
$Pt/\gamma\text{-}Al_2O_3$	1.7% Pt	45.0	1.62	0.036	200.5
$Ni/\gamma\text{-}Al_2O_3$	1.5% Ni	14.4	2.65	0.184	40.1
$PdNi/\gamma\text{-}Al_2O_3$	0.91% Pd, 1.5% Ni	22.3	2.93	0.131	46.5
$PtCo/\gamma\text{-}Al_2O_3$	1.7% Pt, 1.5% Co	35.0	2.51	0.072	245.8
$Co/\gamma\text{-}Al_2O_3$	1.5% Co	6.5	2.12	0.326	73.9

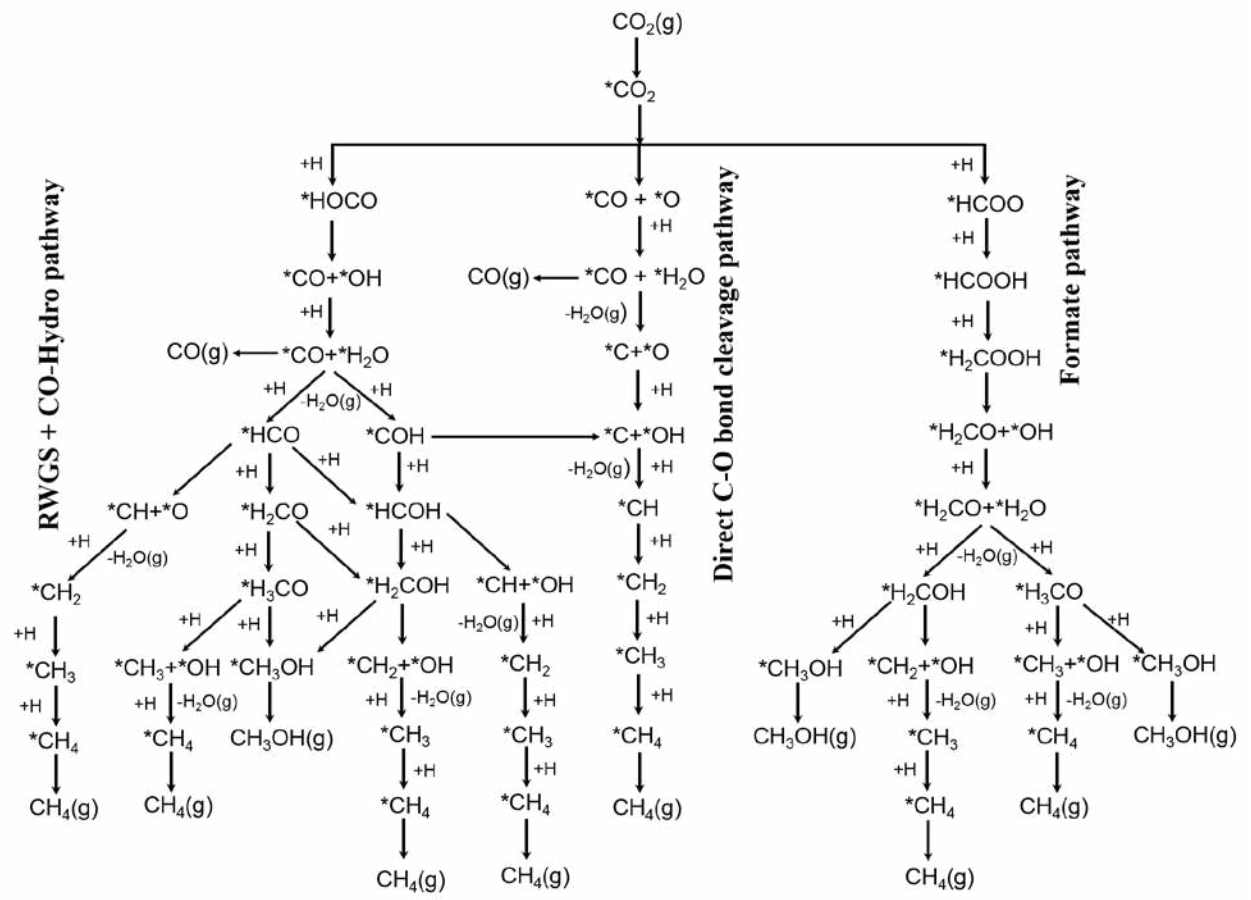

Figure 1. Possible reaction pathways of CO_2 hydrogenation to CO, CH_3OH and CH_4. *(X) indicates adsorbed species.

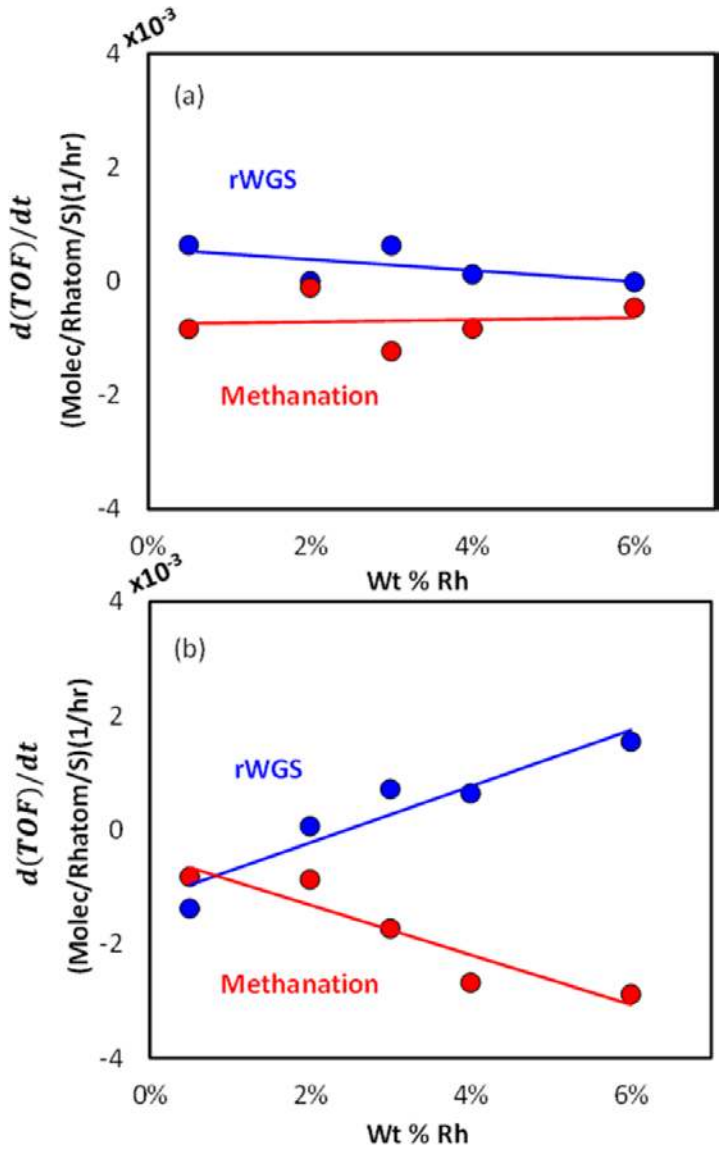

Figure 2. Rate of turn over frequency (TOF) change (d(TOF)/dt) for both reaction pathways as a function of wt % Rh measured at 200 °C and feed ratio of (a) $0.25CO_2$:H_2 and (b) $10CO_2$:H_2. Rates of change for the RWGS TOF are shown in blue points and methanation TOF in red points. The linear fits to the data are added for visual clarity. Reproduced with permission from ref [75]. Copyright 2015 American Chemical Society.

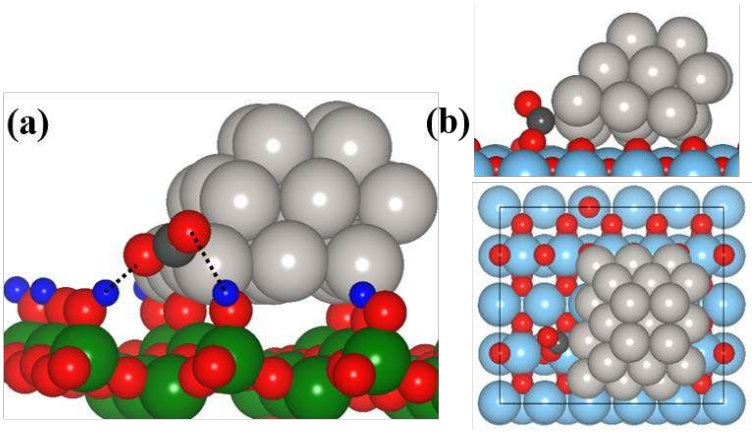

Figure 3. Adsorption geometry of CO_2 on (a) Pt/SiO_2 and (b) Pt/TiO_2. Reproduced with permission from ref [51]. Copyright 2016 Elsevier.

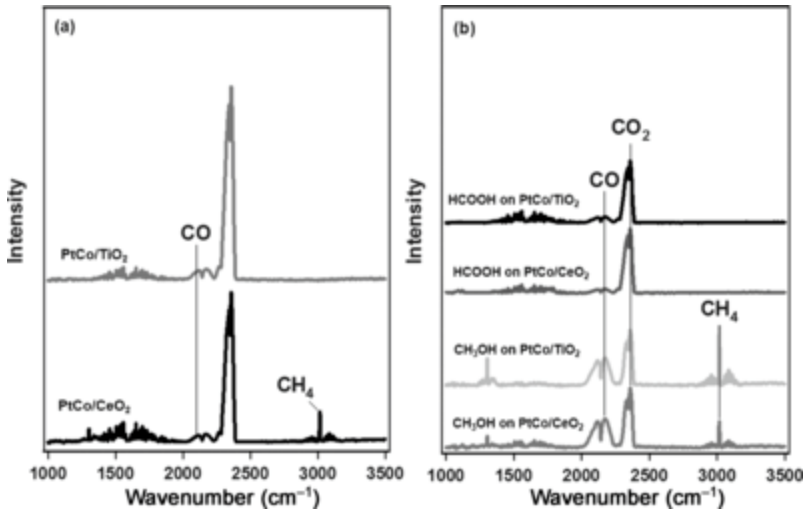

Figure 4. Fourier transform infrared spectroscopy (FTIR) spectra during the reaction of (a) CO_2 reduction by H_2 and (b) formic acid and methanol on $PtCo/CeO_2$ and $PtCo/TiO_2$ catalysts. Reproduced with permission from ref [39]. Copyright 2016 Wiley.

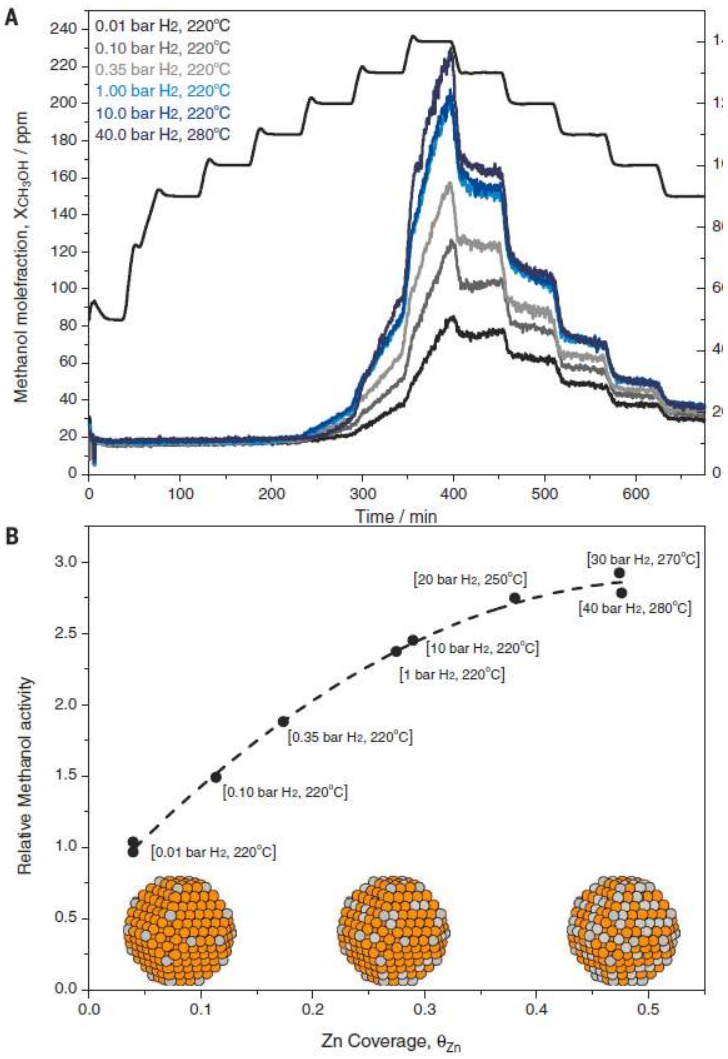

Figure 5. Methanol activities as a function of the Zn coverages at the Cu nanoparticles of a $Cu/ZnO/Al_2O_3$ methanol catalyst. (A) Temperature ramp and exit methanol concentrations after pretreatment as a function of time and temperature in a $CO/CO_2/H_2$ = 18/18/64 gas mixture at ambient pressure and space velocity (SV) = 30 to 33 Nl/g/h. (B) Relative measured methanol exit concentrations at 130 °C (temperature ramp-down) as a function of postreaction values of θ_{Zn}. The varying values of θ_{Zn} are obtained by pretreatments in H_2 at different pressures and temperatures prior to activity tests. The dashed line is a second-order polynomial fit to the data. Reproduced with permission from ref [29]. Copyright 2016 AAAS.

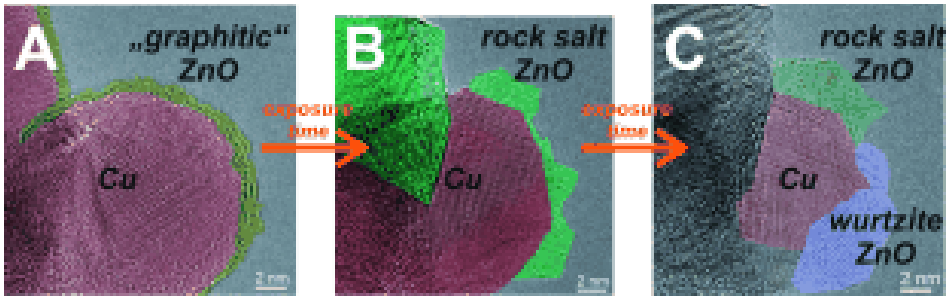

Figure 6. Transformation from graphitic-like ZnO_x to the wurtzite structure. A–C) aberration-corrected high resolution transmission electron microscopy (HRTEM) images of Cu/ZnO/Al_2O_3 after different times of electron beam exposure. For improved assignment of the lattice fringes, the particle in (C) was slightly tilted towards a zone axis of ZnO by 128. The colors indicate the different state during phase transformation. The red-colored sites correspond to Cu particles. Yellow indicates graphitic-like ZnO_x. Green highlights the rock salt ZnO and blue regions correspond to the wurtzite ZnO structure. Reproduced with permission from ref [101]. Copyright 2015 Wiley.

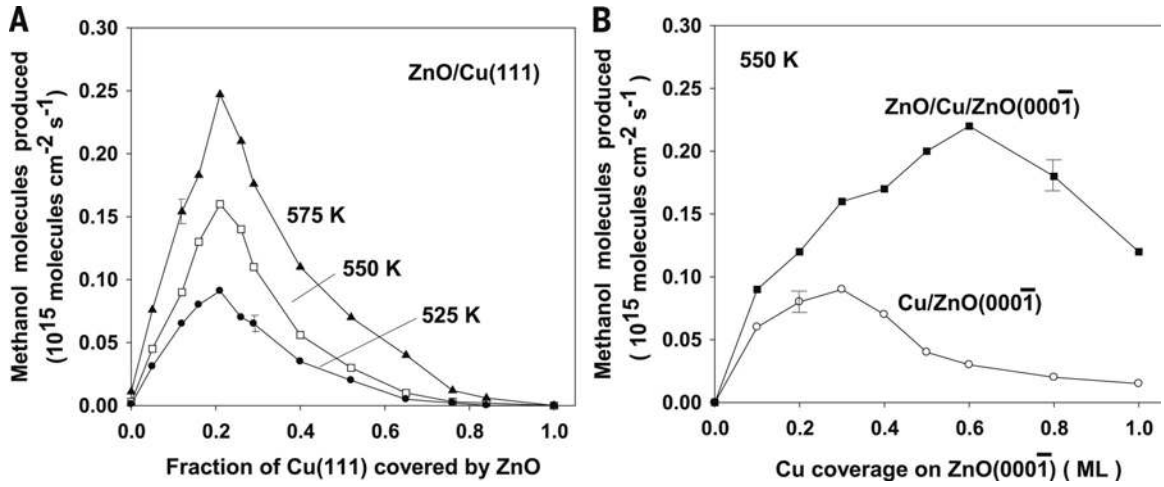

Figure 7. A) Rate for the conversion of CO_2 to methanol on Cu(111) as a function of the fraction of the metal surface covered by zinc oxide. Reaction conditions: T (temperature) = 525, 550, or 575 K; P_{H2} (partial pressure of H_2) = 4.5 atm; P_{CO2} (partial pressure of CO_2) = 0.5 atm. (B) (Bottom trace) Rates for the production of methanol on Cu/ZnO(000$\bar{1}$) surfaces at 550 K, P_{CO2} = 0.5 atm, P_{H2} = 4.5 atm. (Top trace) Rates measured after depositing 0.4 ML of ZnO on the Cu/ZnO(000$\bar{1}$) surfaces. Reproduced with permission from ref [47]. Copyright 2017 AAAS.

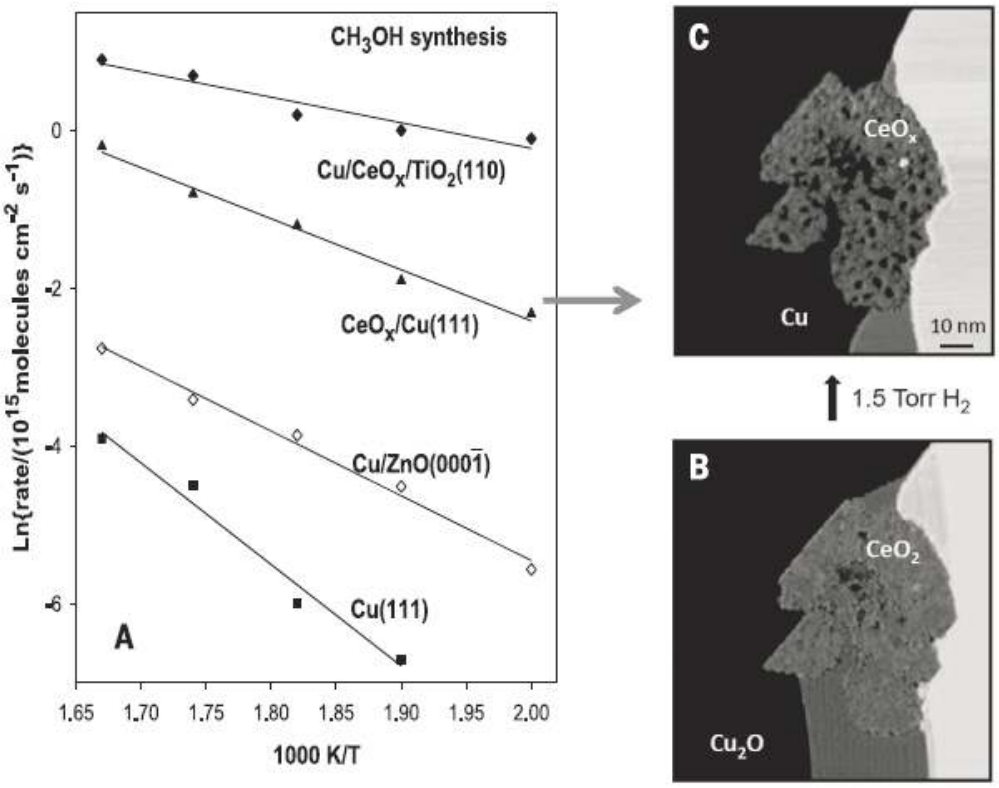

Figure 8. Kinetics and scanning tunneling microscope (STM) studies. (A) Arrhenius plot for methanol synthesis on Cu(111), a 0.2 ML of Cu on ZnO(000$\bar{1}$), a Cu(111) surface covered 20% by ceria, and a 0.1 ML of Cu on a TiO_2(110) surface precovered 15% with ceria. In a batch reactor, the catalysts were exposed to 0.5 atm of CO_2 and 4.5 atm of H_2. The reported values are steady-state rates measured at 600, 575, 550, 525, and 500 K. (B) STM image of a CeO_x/Cu(111) surface as prepared. (C) In situ STM image taken during exposure to 1.5 torr of H_2 at 300 K after 26 hours of reaction. Scanning parameters: 0.3 nA, 1.0 V. Reproduced with permission from ref [28]. Copyright 2014 AAAS.

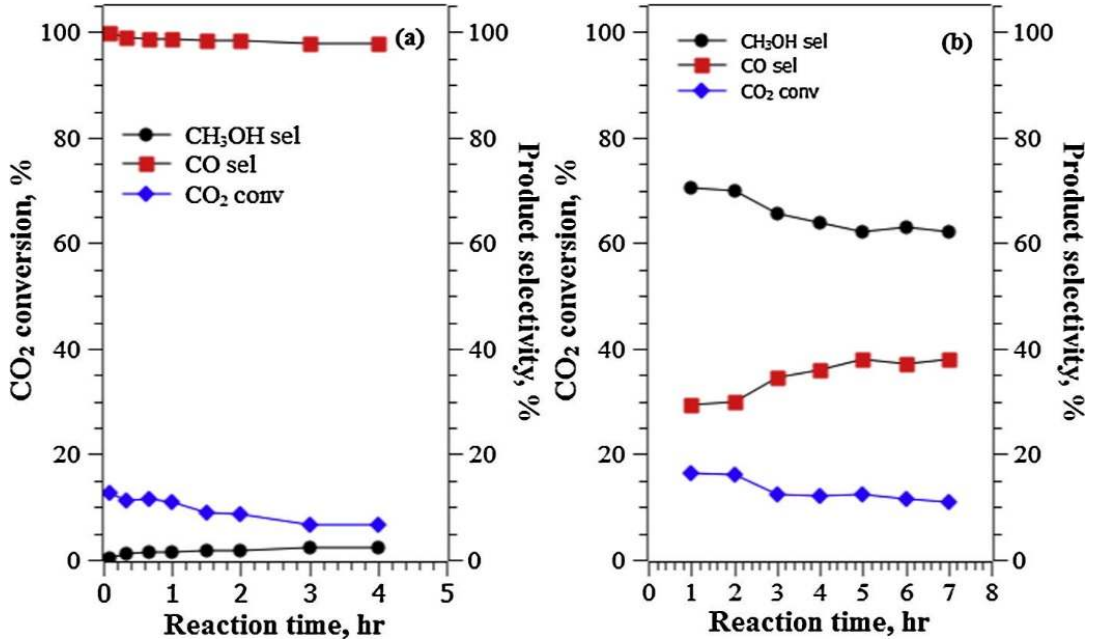

Figure 9. CO_2 hydrogenation reaction on (a) 5% Pd/ZnO by impregnation and (b) 5% Pd/ZnO catalyst prepared by sol immobilization method. The catalysts were pre-reduced prior to the reaction at 400 °C under flow of H_2. The reaction was carried out at 250 °C at 20 bar with $1CO_2$: $3H_2$ at 30 ml/min. Reproduced with permission from ref [99]. Copyright 2016 Elsevier.

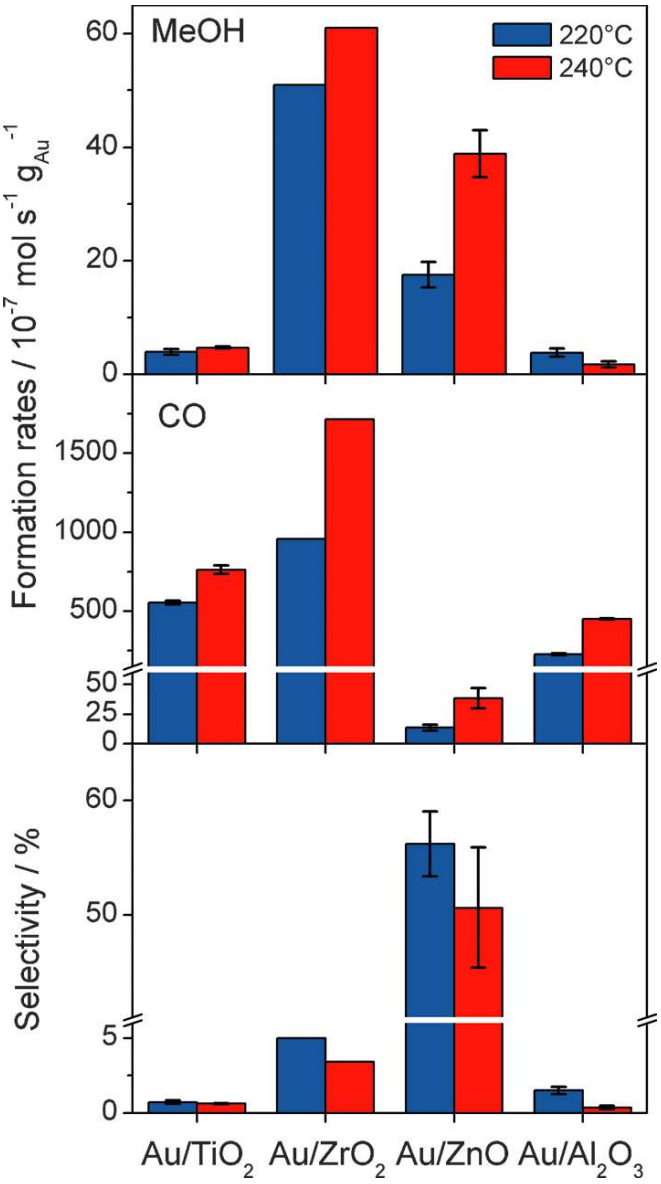

Figure 10. Au mass-normalized formation rates and selectivity for CH_3OH formation during CO_2 hydrogenation at 220–240 ^{0}C and 5 bar in 25% CO_2/rest H_2 over Au catalysts supported on different metal oxides after calcination in 20 NmLmin^{-1} of 1% O_2/N_2 at 400 ^{0}C for 1 h (O400). Error bars represent the standard deviation from several repeat measurements. Reproduced with permission from ref [31]. Copyright 2015 Wiley.

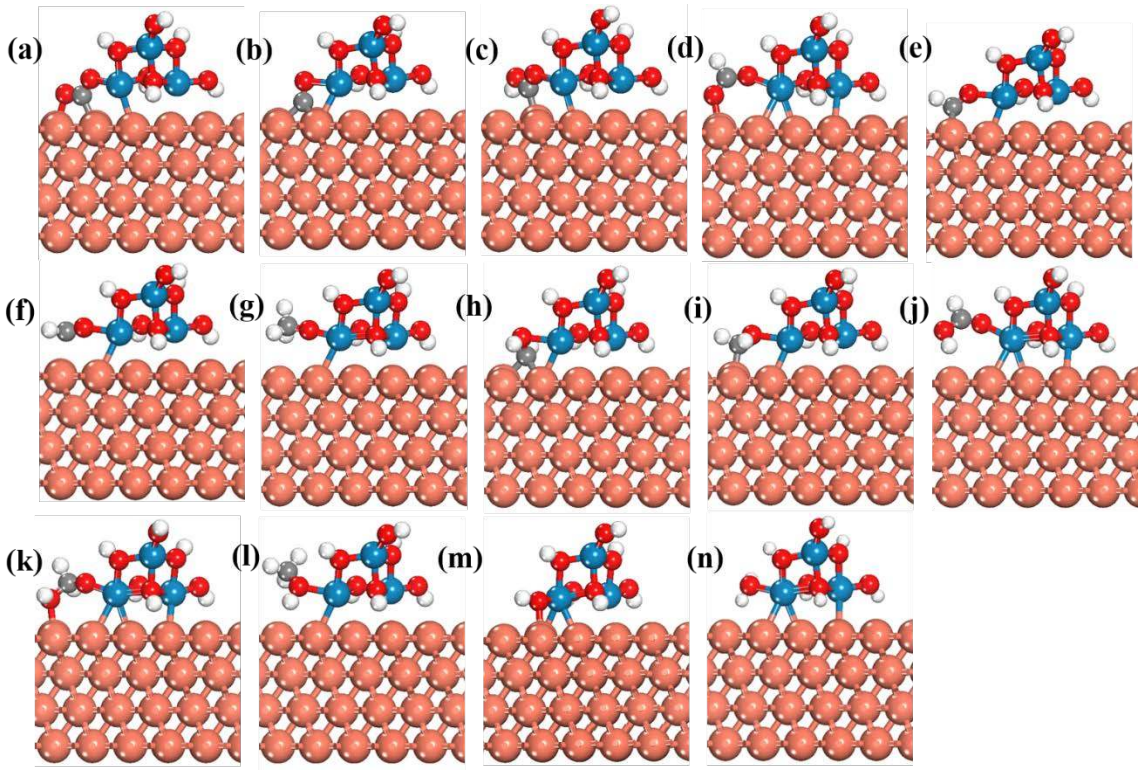

Figure 11. DFT optimized geometries. (a) *CO_2, (b) *CO, (c) *HOCO, (d) *HCOO, (e) *HCO, (f) *H_2CO, (g) *H_3CO, (h) *HCOH, (i) *H_2COH, (j) *HCOOH, (k) *H_2COOH (l) *CH_3OH, (m) *OH and (n) *H_2O on $Ti_3O_6H_6$/Cu(111). Cu: reddish-orange, Ti: blue, O: red, C: grey and H: white. Reproduced with permission from ref [38]. Copyright 2016 American Chemical Society.

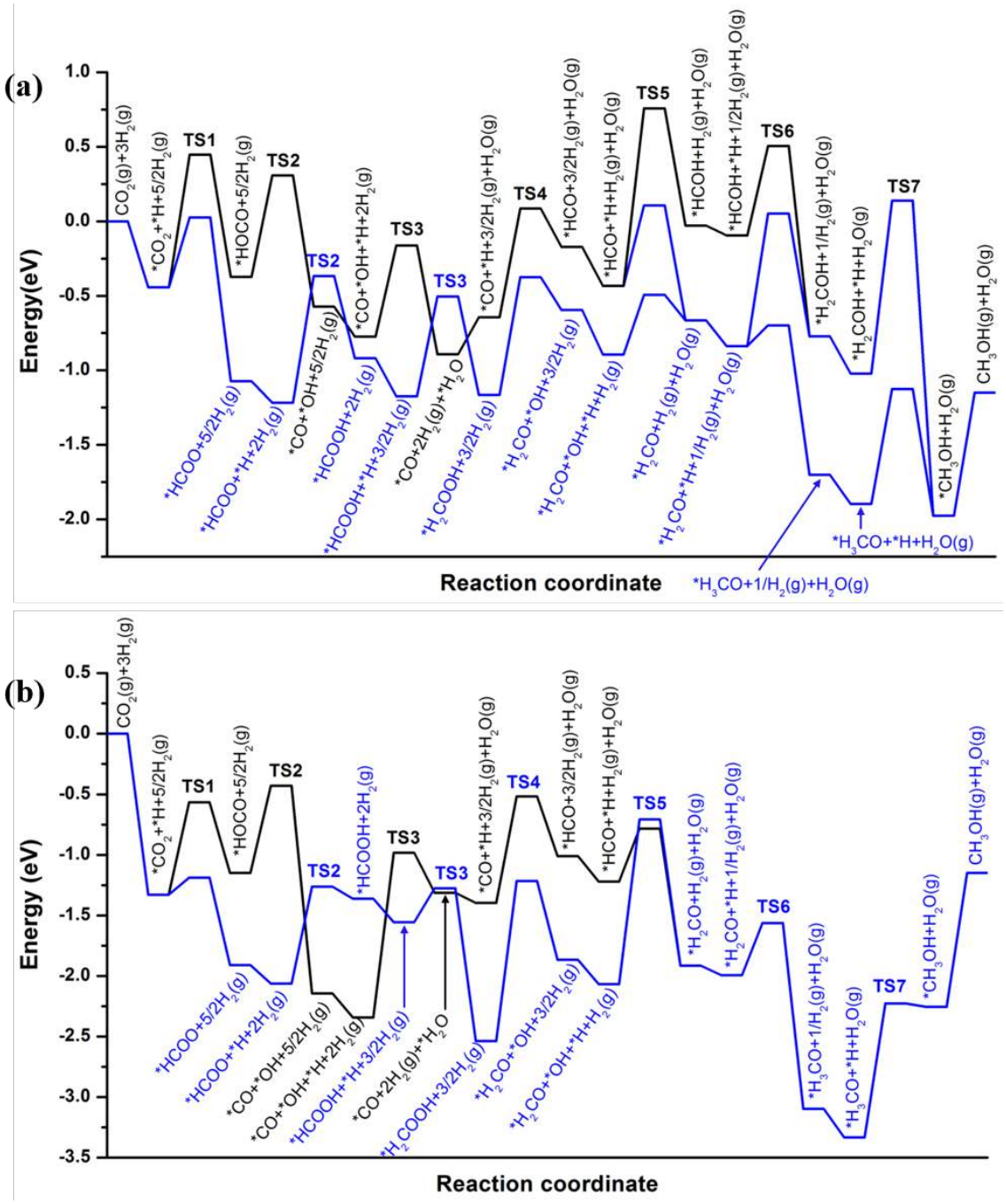

Figure 12. Potential energy diagrams for the hydrogenation of CO_2(g) to CH_3OH(g) on (a) $Ti_3O_6H_6$/Cu(111) and (b) $Zr_3O_6H_6$/Cu(111) via the RWGS + CO-Hydro and Formate pathways. "TS" corresponds to the transition state. Reproduced with permission from ref [38]. Copyright 2016 American Chemical Society.

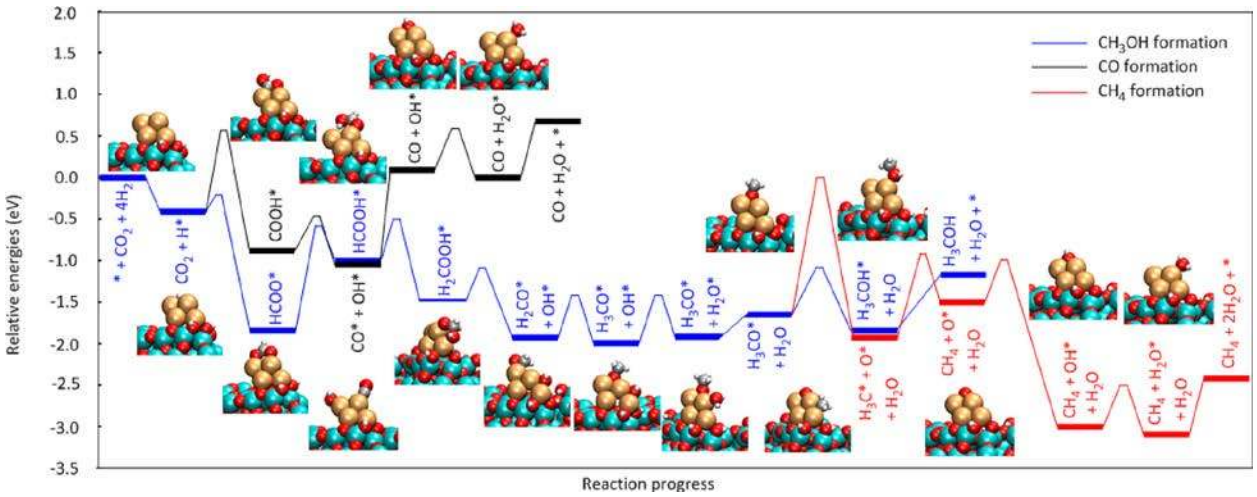

Figure 13. Calculated reaction pathways of CO_2 reduction to CH_3OH, CO and CH_4 on Al_2O_3 supported Cu_4 clusters. To improve legibility, "H_2" was omitted from the labels after the initial state. Reproduced with permission from ref [117]. Copyright 2015 American Chemical Society.

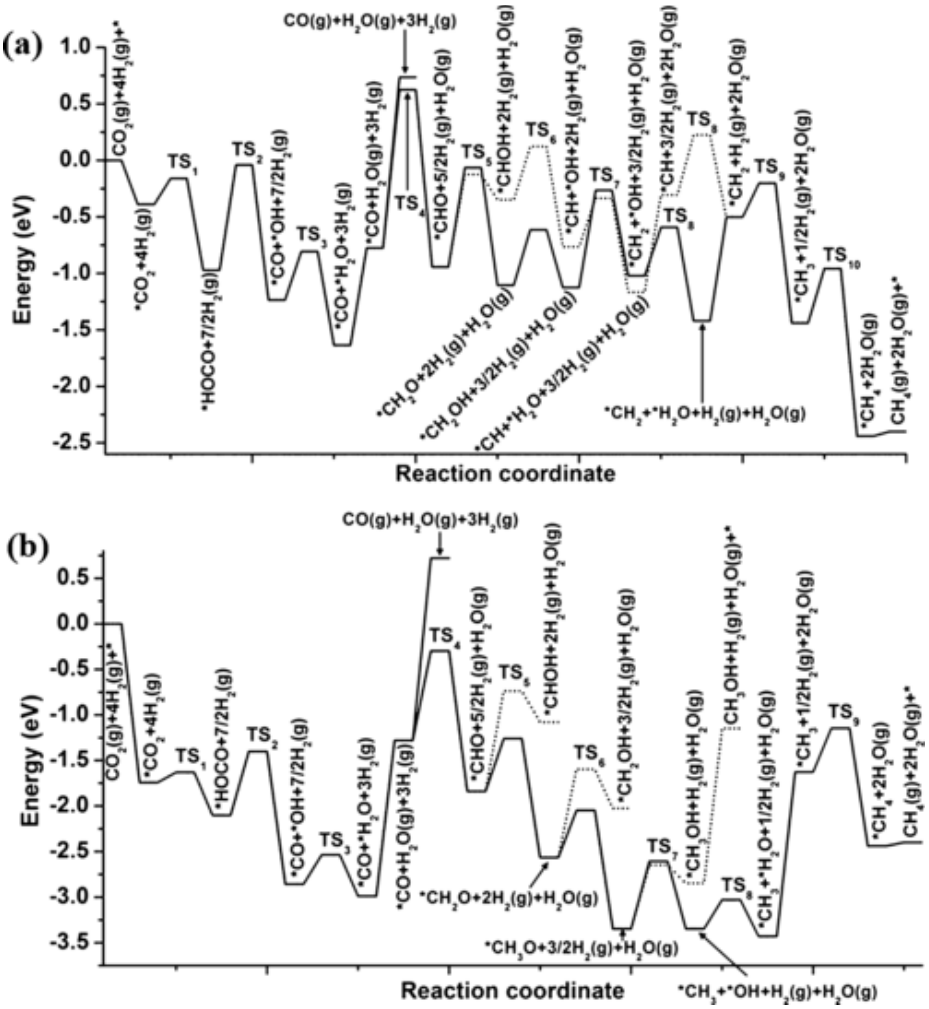

Figure 14. Potential energy diagrams for the CO, and CH_4 synthesis via the RWGS + CO-Hydro pathways on model hydroxylated Ti_3O_6/PtCo(111) (a) and Zr_3O_6/PtCo(111) (b) surfaces. Reproduced with permission from ref [39]. Copyright 2016 Wiley.

TOC